

GAS PHASE METHANOL SYNTHESIS FOR CARBON-11
RADIOPHARMACEUTICALS

by

Erik van Lier

B.Eng., McGill University, May 2001

A THESIS SUBMITTED IN PARTIAL FULFILLMENT OF

THE REQUIREMENTS FOR THE DEGREE OF

MASTER OF APPLIED SCIENCE

in

THE FACULTY OF GRADUATE STUDIES

(Chemical and Biological Engineering)

THE UNIVERSITY OF BRITISH COLUMBIA

August 2007

© Erik van Lier, 2007

Abstract

Carbon-11 radiopharmaceuticals are gaining an increasing importance in positron emission tomography due to their importance in diagnostic medicine. The most wide spread method of production of these radiopharmaceuticals is by methylation of an appropriate precursor with the highly reactive [^{11}C]methyl iodide. Conventional synthesis of this intermediate involves liquid phase synthesis of [^{11}C]methanol, which is the step that limits the specific activity of the final product. A catalytic gas phase methanol synthesis process was evaluated, that promises to avoid the loss of specific activity. In this procedure, [^{11}C]carbon dioxide produced in the target is first trapped and purified, then converted to [^{11}C]carbon monoxide using molybdenum and finally reduced to [^{11}C]methanol using a copper zinc oxide catalyst in the presence of hydrogen.

In this study a device to trap and purify [^{11}C]carbon dioxide was developed and optimized. [^{11}C]Carbon dioxide produced in target was quantitatively trapped at -20°C on a carbon molecular sieve column and quantitatively released in less than 3.5 minutes.

A reactor to convert 50 ppm carbon dioxide to carbon monoxide, based on the reaction with molybdenum, was developed. A commercially available process simulator was used to assist the optimization of operating conditions and molybdenum pretreatment methods. Under optimal conditions, carbon dioxide was converted to carbon monoxide with over 70% yield.

A reactor to catalytically convert 50 ppm carbon monoxide to methanol was developed. A copper zinc oxide catalyst was prepared by a co-precipitation method. The catalyst was

activated by reduction with hydrogen and passivated with compressed air prior to methanol synthesis. The effect of temperature, pressure and flowrate on the conversion of carbon monoxide to methanol were studied and results were used to create a kinetic model. This model was used to determine optimal operating conditions for this reactor and predicts 60% conversion of [^{11}C]carbon monoxide to [^{11}C]methanol.

These findings suggest that gas phase [^{11}C]methanol synthesis is a viable alternative to the conventional liquid phase method, meriting further studies with carbon-11.

Contents

Abstract	ii
Nomenclature	x
Acknowledgements	xv
1 Introduction	1
1.1 Background	1
1.1.1 Positron emission tomography	2
1.1.2 Application of PET	7
1.1.3 Carbon-11 radiopharmaceuticals	8
1.2 Objective of the study	9
2 Literature review	11
2.1 Radiochemistry of carbon-11	11
2.1.1 Production of C-11	12
2.1.2 Recovery and purification of $^{11}\text{CO}_2$ and $^{11}\text{CH}_4$	14
2.1.3 Reduction of $^{11}\text{CO}_2$ and oxidation of $^{11}\text{CH}_4$	17
2.1.4 Synthesis of $^{11}\text{CH}_3\text{OH}$	20
2.1.5 Synthesis of carbon-11 radiopharmaceuticals	22
2.2 Molybdenum compounds for the reduction of CO_2 to CO	23
2.2.1 History	23

2.2.2	Reduction of molybdenum oxides	24
2.2.3	Oxidation of molybdenum	26
2.2.4	Interaction of CO ₂ and CO with Mo ₂ C	27
2.3	Methanol synthesis	30
2.3.1	History	30
2.3.2	Catalyst preparation	31
2.3.3	Catalyst poisoning / deactivation	32
2.3.4	Thermodynamics and kinetics	32
3	Experimental: Trapping and purification of ¹¹CO₂	34
3.1	Introduction	34
3.2	Materials and methods	35
3.3	Experimental set-up	36
3.4	Experimental procedure	36
3.4.1	Production of ¹¹ CO ₂	37
3.4.2	Trapping and release of ¹¹ CO ₂	39
3.5	Results and discussion	40
3.5.1	Effect of carbon molecular sieve mass on ¹¹ CO ₂ trapping efficiency	41
3.5.2	Effect of trap temperature on CO ₂ trapping efficiency	42
3.5.3	Overall trapping efficiency	43
4	Experimental: Reduction of CO₂ to CO	44
4.1	Introduction	44
4.2	Preliminary experiments: reaction of ¹¹ CO ₂ and Mo	44
4.2.1	Materials and methods	44
4.2.2	Experimental set-up	45
4.2.3	Experimental procedure	46
4.2.4	Results and discussion	46

4.3	Equilibrium computer simulations of systems containing molybdenum . . .	48
4.3.1	Reduction of MoO ₃ with H ₂	49
4.3.2	Oxidation of Mo with O ₂	50
4.4	Cold experiments: reaction of CO ₂ and Mo	54
4.4.1	Introduction	54
4.4.2	Materials and methods	55
4.4.3	Experimental set-up	56
4.4.4	Experimental procedure	57
4.4.5	Results and discussion	59
5	Experimental: Methanol synthesis	65
5.1	Introduction	65
5.2	Materials and methods	66
5.2.1	Cu/ZnO catalyst preparation	67
5.3	Experimental procedure	68
5.3.1	Preliminary experiments: Cu/ZnO catalyst for CH ₃ OH synthesis . . .	68
5.3.2	Effect of flowrate and temperature on CH ₃ OH synthesis	69
5.4	Results and discussion:	71
5.4.1	Preliminary experiments: Cu/ZnO catalyst	71
5.4.2	Effect of flowrate and temperature on CH ₃ OH synthesis	73
5.4.3	Kinetic Model	76
6	Conclusion and Recommendations	80
6.1	Conclusions	80
6.2	Recommendations for future work	81
	Bibliography	83

Appendices	91
Appendix I: Flowmeter calibration curves	91
Appendix II: Calibration curves	93
Appendix III: Surface molybdenum	96
Appendix IV: Temperature profile	98
Appendix V: Process simulator	100
Appendix VI: Carbon dioxide estimate	105

List of Tables

3.1	C-11 target yields, 14 MeV	40
3.2	$^{11}\text{CO}_2$ trapping/releasing Sequence	41
3.3	$^{11}\text{CO}_2$ trapping efficiencies	41
3.4	Comparison of overall trapping efficiency	43
4.1	$^{11}\text{CO}_2$ Reduction sequence	47
4.2	Summary of ^{11}CO yields, 17.5-70 cm^3/min , 2 bar	47
5.1	Effect of flowrate on conversion of CO to methanol (50bar, 180°C)	74
5.2	Effect of temperature on conversion of CO to methanol at 55bar, 126 $\text{cm}^3/\text{min}(\text{STP})$	74
5.3	Kinetic parameters for Leonov's model	76
6.1	Mo surface moles rough estimate	96
6.2	Mo total moles	97
6.3	CO_2 concentration estimates	105

List of Figures

1.1	Conceptual visualization of a cyclotron	3
1.2	Interior view of the PET TR-19 cyclotron	4
1.3	Annihilation of a positron	5
1.4	Commercial PET scanner	6
1.5	^{18}F FDG-PET scan of a breast cancer patient	7
2.1	Separation of air, CO, CH ₄ and CO ₂ using gas chromatography	17
2.2	Separation of H ₂ , air, CH ₄ and CO ₂ using gas chromatography	18
2.3	Decay corrected ^{11}C yields as a function of temperature	28
2.4	CO formation rate from temperature programmed reaction of CO ₂ with Mo ₂ C	29
3.1	^{11}C CO ₂ Trapping experimental flow diagram	37
3.2	^{11}C CO ₂ activity vs. time, for different trap temperatures.	42
4.1	^{11}C CO ₂ Reduction experimental flow diagram	45
4.2	Equilibrium compositions of Mo-MoO-MoO ₂ -MoO ₃ -H ₂ -O ₂ -H ₂ O from 300 to 1500 K	50
4.3	Equilibrium mole fraction of MoO ₂ for different H ₂ :MoO ₃ ratios from 300 to 1500K	51
4.4	Equilibrium of composition of Mo-MoO ₂ -Mo ₂ C-CO ₂ -CO	52
4.5	Equilibrium molar fraction of CO ₂ from eqs. 4.5	53
4.6	Equilibrium molar fraction of CO from eqs. 4.6	53

4.7	Conversion of CO ₂ to CO vs. temperature for different CO ₂ concentration, based on Aspen equilibrium data	54
4.8	Experimental flow-diagram for the reduction of CO ₂	57
4.9	Effect of temperature on reaction of CO ₂ and Mo, at 4 cm ³ /min and 2 bar .	60
4.10	Effect of flowrate on reaction of CO ₂ and Mo at 825°C and 2 bar	61
4.11	Total carbon oxides as a function of temperature.	62
4.12	Total carbon oxides as a function of flowrate.	62
5.1	Experimental flow diagram for methanol synthesis	68
5.2	Aspen generated equilibrium conversion of 50 ppm CO to methanol, in hydrogen	69
5.3	Methanol produced for continuous feed of H ₂ /CO	72
5.4	Semi-batch methanol produced, 180°C, 50 bar for different flowrates . . .	73
5.5	Semi-batch methanol produced, 120 cm ³ /min, 50 bar for different temper- atures	75
5.6	Conversion of carbon monoxide to methanol vs. temperature	77
5.7	Conversion of carbon monoxide to methanol vs. flowrate	78
6.1	Mass flow control valve calibration curve	92
6.2	Correlated ball flowmeter calibration curve	92
6.3	Gas chromatogram of CO containing sample	94
6.4	CO ₂ , CO and CH ₃ OH calibration curves	95
6.5	Reactor temperature profile, at 740°C	99
6.6	Equilibrium relationships at atmospheric pressure Mo-C-Mo ₂ C-H ₂ -CH ₄ . .	101
6.7	Aspen generated equilibrium relationships at atmospheric pressure Mo-C- Mo ₂ C-H ₂ -CH ₄	102

Nomenclature

α	Alpha particle: 2 protons and 2 neutrons
ϕ	Diameter
ξ_T	Trapping Efficiency, ratio of the amount of C-11 trapped to the amount of C-11 entering the trap
ξ_T	Recovery Efficiency, ratio of the amount of C-11 released from the trap to the amount of C-11 released from the target
A	Mass number: number of protons + number of neutrons
<i>i.d.</i>	Inner Diameter
l	Length
N	Activity remaining after initial activity N_0 has decay for time t
N_0	Initial amount of activity
<i>o.d.</i>	Outer Diameter
P_e	Particle emitted
P_i	Incident Particle
p	Proton

t	Synthesis time, minutes
$t_{1/2}$	Half life: 20.4 minutes for ^{11}C
t_T	Trap time: time elapsed between begin of target unloading until C-11 is recovered from the trap
TPR	Temperature Programmed Reduction
X	Target Nucleus
X'	Residual Nucleus
y	Yield, defined as the amount of final product (mCi) divided by the amount of starting material (mCi)
y'	Decay corrected yield, defined as the yield assuming no decay of product occurred
Z	Atomic number: number of protons
mCi	MilliCuries, unit of radioactivity defined to be the decay rate of 1.00 g radium, which corresponds to 37 billion disintegrations per second
CCH ₃ OH	Concentration methanol, ppm
CCO	Concentration carbon monoxide, ppm
CCO ₂	Concentration carbon dioxide, ppm
E_a	Activation energy
EOB	End of Bombardment
F	Flowrate, gas flowrate defined in standard cubic centimeters per minute
FID	Flame Ionization Detector

I Proton beam intensity, in microamperes

IBS Ion Beam Stop

id Inner Diameter

k Reaction rate constant

Keq Equilibrium constant

ko Reaction rate pre-exponential factor

LiAlH₄ Lithium aluminum hydride

n Number of experiments repeated at same conditions

od Outer Diameter

PET Positron Emission Tomography

P_i Component i partial pressure

R Ideal gas law constant

r Methanol formation reaction rate

STDEV Standard Deviation

STP Standard Temperature and Pressure

T Temperature

TEC Thermo Electric Cooler

THF Tetrahydrofuran

TPR Temperature Programmed Reduction

UHP Ultra High Purity

Vi Input Voltage, defined as the input voltage signal supplied to the mass flow controller, in volts

Acknowledgments

I would like to thank my supervisors at UBC, Dr's. Dusko Posarac, C.J. Lim and E. Kwok, as well as my mentors at Ebco Technologies Inc., Dr's. R. Johnson and K. Erdman, for their guidance and support. I also would like to thank my colleagues at Ebco Technologies and Advanced Cyclotron Systems Inc. and fellow students and machine shop from the Department of Chemical and Biological Engineering for their assistance with technical issues and their continued support. Finally, I would like to acknowledge the Science Council of British Columbia, National Science and Engineering Research Council of Canada and Ebco Technologies for making this project possible. Finally, I would like to thank my family for their support.

Chapter 1

Introduction

1.1 Background

Short half-life radiopharmaceuticals are used in nuclear medicine together with positron emission tomography (PET) cameras to visualize organ function, particularly of the brain and the heart. PET clinics routinely use radiopharmaceuticals as a diagnostic tool for various disease conditions including cancer. Since the early 1970's, the number of radiopharmaceuticals labeled with the positron-emitting radionuclide carbon-11, has rapidly increased. The most widely used carbon-11 labeling method involves methylation of an appropriate precursor, using [^{11}C]methyl iodide as an intermediate [1].

For many medical applications it is essential that the radiopharmaceutical possesses a high specific activity [2], i.e. a high concentration of radioactivity per unit mass. The process for production should permit sequential automated production runs, while minimizing operator exposure to radiation. Producing high specific activity [^{11}C]methyl iodide with sufficient yield has been one of the major challenges in developing a process for the routine production of carbon-11 radiopharmaceuticals [3, 4].

1.1.1 Positron emission tomography

The in vivo study of biochemical processes, i.e. molecular imaging, became a reality in the second half of the 20th century [5, 6]. Discoveries made in nuclear physics in the 1930's gave rise to the conceptual idea of measuring biochemistry in vivo [7, 8]. Although radioisotopes could be produced, there were several technological barriers preventing the transfer of this technology to a clinical setting. Scintillation crystals were discovered around 1950 [9] and computers for data acquisition and processing were only available at a later date. The first positron camera was constructed in the 1960s [10]. Ten years later, groups in Europe, Japan and North America produced PET radiopharmaceuticals and developed PET scanners[10].

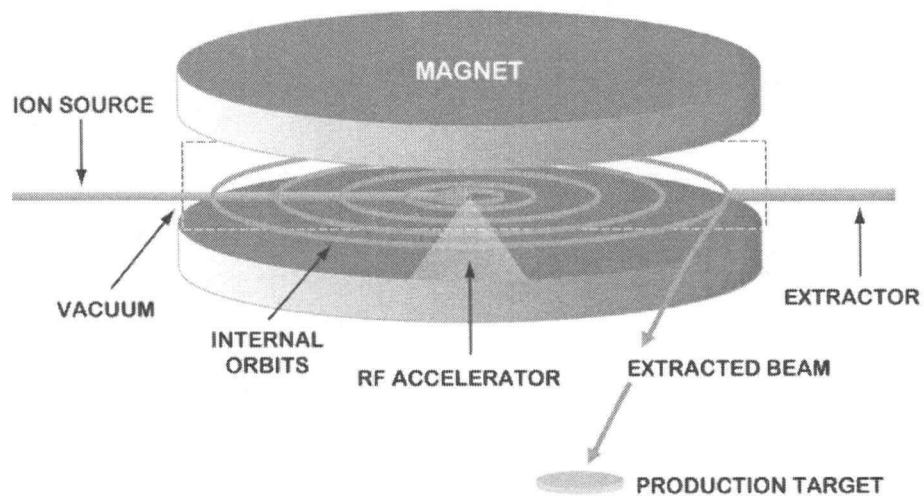
The major steps involved in PET imaging are production of the radioisotope with a particle accelerator, synthesis of the appropriate radiopharmaceutical and in vivo visualization of the biological uptake with 3-dimensional PET scanners.

Particle accelerators

The first step in PET is the production of the appropriate radionuclide by bombarding a target material with accelerated protons or deuterons. This can be accomplished using a linear accelerator or a cyclotron; most PET facilities use a cyclotron due to lower overall cost and physical size. In a linear accelerator, particles travel down a long, straight track and collide with the target. In a cyclotron, particles travel in a circular orbit until they reach the required energy and collide with a target.

A conceptual visualization of a cyclotron is illustrated in Figure 1.1. It consists of a pair of hollow, semicircular metal electrodes (dee's), positioned between the poles of a large magnet. The dee's are separated from one another by a narrow gap and enclosed in a high vacuum chamber.

An external source of ions (typically H^+) supplies charged particles to the center of the cyclotron. As they enter the cyclotron, the radio-frequency (RF) accelerator alternates the



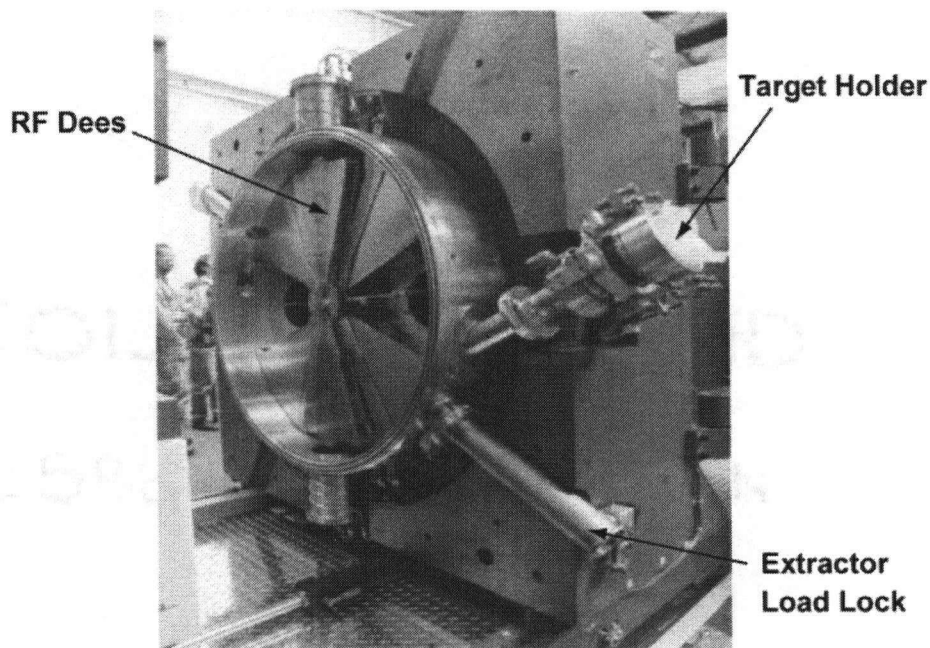
Courtesy of Ebco Technologies Inc. [11]

Figure 1.1: Conceptual visualization of a cyclotron

electric field between the dee's within the cyclotron. The incoming ions are exposed to this electric field as well as a strong magnetic field generated by the main magnet, accelerating the negative ions in a circular path. As the number of orbits increases, so does their speed and energy. When the desired energy is reached, the electrons are stripped off the negatively charged ions by a carbon extraction foil, and the resulting positive ion beam is thus extracted from its orbit. The resulting proton (or deuteron) beam collides with the target material to produce the desired radioisotope. Figure 1.2 illustrates a modern cyclotron, with the main vacuum chamber open.

Radioisotope production

A general form to describe a nuclear reaction between the target material and the accelerated proton or deuteron is shown in eq. 1.1 [12], where X is the target material, P_i is the incident particle, X' the generated radioisotope, and P_e the emitted particle.



Courtesy of Ebco Technologies Inc. [11]

Figure 1.2: Interior view of the PET TR-19 cyclotron



The production of carbon-11 (eq. 1.2) involves the bombardment of nitrogen gas with an incident beam of protons, which creates a very unstable oxygen-15 intermediate [13] containing 8 protons and 7 neutrons. This intermediate instantaneously stabilizes by emitting an alpha particle (2 protons, 2 neutrons), to yield the radionuclide carbon-11, which has 6 protons and 5 neutrons.

Common radionuclides produced with a medical cyclotron are ${}^{11}C$ ($t_{1/2} = 20.4$ min), ${}^{13}N$ ($t_{1/2} = 10$ min), ${}^{15}O$ ($t_{1/2} = 2$ min) and ${}^{18}F$ ($t_{1/2} = 110$ min). These radionuclides decay by pure positron emission, as illustrated by the decay of carbon-11 in eq. 1.3. The half life is a characteristic constant for a given radioisotopes and corresponds to the time

required for half of a radioactive sample to decay [14].



In addition to their short half lives, the principal positron emitters ${}^{11}\text{C}$, ${}^{13}\text{N}$, ${}^{15}\text{O}$ and ${}^{18}\text{F}$ are useful for clinical PET since their stable isotopes are the building blocks for most organic molecules (${}^{18}\text{F}$ is used in place of H or OH). The radionuclides are chemically processed to prepare a radiopharmaceutical that will target the desired metabolic process or tissue in the body.

PET Cameras

Positrons (β^{+}) travel at most a few millimeters before they are annihilated with nearby electrons to give two gamma rays of 511 keV emitted in opposite directions (Figure 1.3).

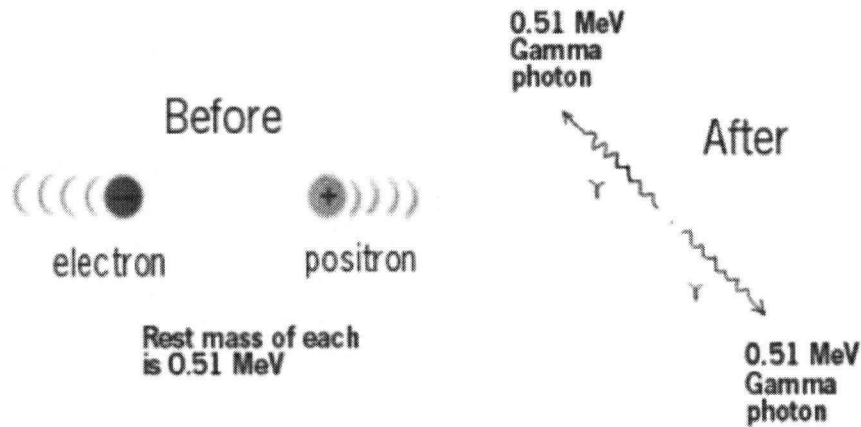


Figure 1.3: Annihilation of a positron

The PET camera uses rings of detectors that register the 511 keV rays from a single annihilation. The detectors are arranged in a circle around the patient, or in a hexagonal array where the detectors are grouped into cassettes. The content of each cassette varies

according to the manufacturer, but usually these consist of 256 scintillating crystals being viewed by 16 photomultiplier tubes (four blocks composed of 64 crystals and four photomultiplier tubes) with as many as three rings of 16 buckets in a circle (12,288 crystals with 768 photomultiplier tubes) [15]. An alternative design to the bucket, is one that uses rings of detectors with 11 crystals in a staggered array being exposed to 6 photomultiplier tubes [15]. As can be seen in Figure 1.4, once the patient is placed inside the scanner, he/she slowly moves through the rings of detectors to provide a whole or partial body scan.



Figure 1.4: Commercial PET scanner

When two detectors at opposite sides of the camera simultaneously detect a gamma ray, the data processor assumes that on the virtual line connecting the two detectors a positron was annihilated. Once sufficient data is collected, a 3-dimensional image of the radiation distribution can be generated. For example, Figure 1.5 shows the ^{18}F FDG uptake in a patient with breast cancer, revealing that numerous active metastatic cancer sites are present.



Courtesy Dr. F. Benard

Figure 1.5: ^{18}F FDG-PET scan of a breast cancer patient

1.1.2 Application of PET

PET is currently used clinically in cardiology, neurology, and oncology. The most common radiopharmaceutical used in PET is ^{18}F fluoro-deoxy-glucose (FDG) [16], which allows the measurement of glucose consumption in vivo and detects organs and tissues with high metabolic activity. Applications of PET in cardiology also include measurement of blood flow with $^{13}\text{NH}_3$ and/or ^{11}C acetate, in addition to the studies on the glucose consumptions of the heart with ^{18}F FDG [17]. Applications in neuroscience include glucose metabolism with ^{18}F FDG, protein synthesis rate with ^{11}C tyrosine and blood flow with H_2^{15}O [18]. In oncology, ^{18}F FDG-PET is a major tool for diagnostic and treatment follow-up. In addition to FDG, ^{11}C methionine, ^{11}C thymine, ^{11}C cytostatics are used for imaging of more specific cancers.

Positron emitter labeling with carbon-11, nitrogen-13 and oxygen-15, can be used to investigate the catalytic processes and to quantify reaction phenomenon, yielding insight in

elementary reaction mechanisms useful as input to mathematical simulations [19].

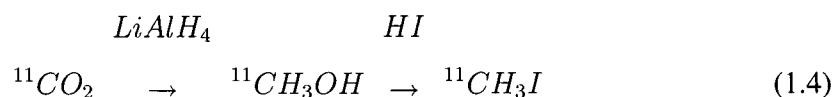
1.1.3 Carbon-11 radiopharmaceuticals

Carbon-11 radiopharmaceuticals are finding an increasing number of applications in cardiology, neurology, and oncology [18]. Many applications, such as brain imaging, require high specific activity radiopharmaceuticals. For example, [^{11}C]raclopride, which is used to visualize dopamine receptors in the brain, requires a high specific activity since only a small number of dopamine receptors are available. Low specific activity, i.e. the presence of many [^{12}C]raclopride molecules, may result in receptor saturation and poor image quality. Many [^{11}C]radiopharmaceuticals are synthesized by the methylation of an appropriate precursor with [^{11}C]methyl iodide, which in turn is generally prepared from [^{11}C]methanol.

Production of carbon-11 radiopharmaceuticals

Carbon-11 is produced in a cyclotron by the bombardment of a gas target filled with nitrogen, using a proton beam (typically 10-19 MeV), via the $^{14}\text{N}(p,\alpha)^{11}\text{C}$ nuclear reaction. In the presence of O_2 , the carbon-11 is produced as $^{11}\text{CO}_2$, while in the presence of H_2 , $^{11}\text{CH}_4$ is produced. A sequence of chemical reactions is carried out to convert these precursors to a carbon-11 radiopharmaceutical, typically via the [^{11}C]CH₃OH and [^{11}C]CH₃I intermediates.

The conventional synthesis of [^{11}C]methyl iodide most widely used over the past 30 years [20] involves two main reactions: the reduction of $^{11}\text{CO}_2$ to $^{11}\text{CH}_3\text{OH}$, followed by iodination to yield $^{11}\text{CH}_3\text{I}$ (eq. 1.4) [20].



In the liquid phase synthesis, $^{11}\text{CO}_2$ is bubbled through a solution of lithium aluminum

hydride (LiAlH_4) for the production of $^{11}\text{CH}_3\text{OH}$, which is then treated with HI to yield $^{11}\text{CH}_3\text{I}$. The LiAlH_4 is a strong reducing agent and is readily contaminated with CO_2 from the atmosphere during preparation of the reagent. Consequently, relatively low specific activity [^{11}C]methyl iodide is generally produced. The quantity of LiAlH_4 utilized in the reaction has a great influence on the yield and specific activity of $^{11}\text{CH}_3\text{OH}$ [13]. Large quantities of LiAlH_4 in the reactor give rise to high yields with low specific activity. On the other hand, small amounts of LiAlH_4 lead to low yields but with higher specific activity. Thus, the main drawback of this method is that a sufficient yield cannot be obtained while simultaneously achieving a high specific activity.

Alternative methods, include the gas phase production of [^{11}C]methyl iodide by reacting $^{11}\text{CH}_4$ with I_2 [21, 22]. This synthesis route avoids the use of LiAlH_4 and consists of recirculating $^{11}\text{CH}_4$ with iodine vapor through a hot reactor.

1.2 Objective of the study

The conventional method to produce many carbon-11 radiopharmaceuticals involves the LiAlH_4 reduction of $^{11}\text{CO}_2$ and is not suitable for production of high specific activity radiopharmaceuticals. The main objective of this study was to determine the feasibility of an alternative gas phase process involving catalytic methanol synthesis, which providing a process for the production of large quantities of high specific activity carbon-11 radiopharmaceuticals.

The proposed gas phase reaction route consists of the reduction of CO_2 to CO followed by catalytic reduction of CO to CH_3OH .

The steps leading to methanol synthesis will be developed and optimized.

Detailed objectives of the present study include:

1. To design / implement / optimize performance of CO_2 trapping device
2. To design / implement / optimize performance of reduction of CO_2 to CO

3. To design / implement / optimize performance of reduction of CO to CH₃OH
4. To develop an empirical rate equation for methanol synthesis to predict performance using carbon-11

Chapter 2

Literature review

This chapter is divided in three sections. The first section deals with the radiochemistry of carbon-11. The second section provides in depth information of the reactions of carbon oxides and molybdenum compounds. The third section includes history and background information on industrial methanol synthesis.

2.1 Radiochemistry of carbon-11

Since the early 1970's, when medical cyclotrons were introduced, an increasing number of compounds are labeled with the positron emitting radionuclide carbon-11 [23]. The most widely used method to produce carbon-11 radiopharmaceuticals involves the methylation of an appropriate precursor with [^{11}C]methyl iodide [2]. Based on this method, a large number of receptor-ligands have been investigated [24]. These radiopharmaceuticals require a high specific activity and it is thus important that each step in their production minimizes contamination with carrier carbon-12.

The conventional method for the preparation of [^{11}C]methyl iodide is the reduction of [^{11}C]carbon dioxide to [^{11}C]methanol by lithium aluminum hydride, followed by conversion to [^{11}C]methyl iodide with hydroiodic acid [25]. An alternative method used by many PET centers involves a recently developed gas phase method, which consists of reacting

[¹¹C]methane with iodine vapor to give [¹¹C]methyl iodide [21, 22, 26].

Throughout this work the terms yield and decay corrected yield are frequently used. The yield is defined as the ratio of the amount of radioactive product to the amount of radioactive starting material, as shown in eq. 2.1. Although synthesis time does not show up directly in this equation, it is incorporated in the yield since a certain amount of C-11 is lost due to decay during the synthesis. However, in order to quantify the efficiency of the various steps in the process, it is desirable to calculate the decay corrected yield, also referred to as the radiochemical yield. It is calculated by multiplying the yield by a decay correction factor, which depends on the time elapsed and the half life of the radionuclide in question, as shown in eq.2.2. The decay corrected yield refers to the yield assuming no radioactive decay occurred, and is also referred to as the chemical yield.

$$y = \frac{\text{Amount Product (mCi)}}{\text{Amount of Reagent (mCi)}} \quad (2.1)$$

$$y' = y \cdot \exp^{0.693 \cdot t/t_{1/2}} \quad (2.2)$$

For example, consider a process which has a 30% yield (¹¹CO₂ to ¹¹CH₃OH) with synthesis time of 20.4 minutes. Since the half life of carbon-11 is 20.4 minutes, the decay corrected yield is 60%. Thus the actual chemical conversion of [¹¹C]carbon dioxide to [¹¹C]methanol is 60%, but since half of the carbon-11 decayed, the actual yield is only 30%.

2.1.1 Production of C-11

Although several nuclear reactions can be used to produce carbon-11, the most convenient is the ¹⁴N(p,α)¹¹C reaction using natural occurring nitrogen gas. Carbon-11 can be produced in the gas target as ¹¹CO₂ or ¹¹CH₄; in the case of ¹¹CO₂ 0.1-2% oxygen is added to the nitrogen, while for ¹¹CH₄ production 5-10% hydrogen is added to the nitrogen gas.

The natural abundance of CO₂ in the air is 330 ppm, whereas that of methane is 1.6 ppm.

This means that much precaution must be taken to exclude air from synthesis modules and reagents during synthesis with $^{11}\text{CO}_2$. However, specific activities of $^{11}\text{CO}_2$ and $^{11}\text{CH}_4$ produced in target are reported to be similar. For in target production of $^{11}\text{CH}_4$, a specific activity of 5 Ci/ μmol was reported [27, 28]. For in target production of $^{11}\text{CO}_2$, specific activities up to 16.5 Ci/ μmol were reported [29]. An independent study demonstrated that only a negligible amount of carrier $^{12}\text{CO}_2$ originates from the target [24]. [^{11}C]Methane production yields are typically less than 65% of [^{11}C]carbon dioxide yields [28]. These factors are among the reasons that many PET centers routinely produce $^{11}\text{CO}_2$ as opposed to $^{11}\text{CH}_4$.

Target for C-11 production

Pure aluminum, aluminum alloys and stainless steel are suitable materials for target construction. Havar[®], titanium or stainless steel are suitable materials for the target window foils. Metal gaskets are preferable to rubber O-rings [13]. In order to reduce potential carrier carbon and increase specific activity, ultra-pure materials with very low carbon content should be used. Thus, ultra pure aluminum would be suitable as target body and ultra pure titanium foil for the target window. For good recovery of C-11 from the target, it is recommended that newly constructed targets be carefully washed with phosphoric acid followed by water, and dried under vacuum.

The target gas should be of high purity and in particular as free as possible from carbon-containing impurities. An additional precaution against [^{12}C]carbon dioxide contamination would be to introduce a carbon dioxide trap in between the nitrogen gas cylinder and the target and also to use stainless steel tubing to minimize entry of carrier $^{12}\text{CO}_2$ by diffusion [13].

$$y^{11}\text{CO}_2 = \frac{^{11}\text{CO}_2 \text{ Produced(EOB)}}{I \cdot (1 - \exp(-0.693 \cdot t/t_{1/2}))} \quad (2.3)$$

An important characteristic for a target is the $^{11}\text{CO}_2$ yield at the end of bombardment (EOB). As can be seen in eq. 2.3, the $^{11}\text{CO}_2$ yield depends on the amount of $^{11}\text{CO}_2$ produced in the target, the half life of C-11, the beam intensity (I) and the duration of irradiation (t). For an energy beam of 14 MeV, C-11 experimental target yields vary between 93 and 135 $\mu\text{Ci}/\mu\text{A}$ [30, 31, 32]. The theoretical target yield, calculated from $^{14}\text{N}(p,n)^{11}\text{C}$ excitation function, was determined to be 169 $\mu\text{Ci}/\mu\text{A}$ at 14 MeV [31]. As can be seen from this data, the reported experimental yields are at least 25% less than the theoretical yield.

2.1.2 Recovery and purification of $^{11}\text{CO}_2$ and $^{11}\text{CH}_4$

The target gas is either a mixture of N_2/H_2 or of N_2/O_2 . The short half life of C-11 makes it necessary to concentrate it rapidly from a large volume of target gas in order to prepare the C-11 radiopharmaceutical [33]. In addition, the carbon-11 produced in the target as $^{11}\text{CO}_2$ or $^{11}\text{CH}_4$ must be separated from the target gas, in order to remove the O_2 or the H_2 , which can affect downstream processing of the C-11 radiopharmaceutical [34]. Two common methods exist for recovery of C-11, which are the use of a cryogenic trap and/or the use of an adsorbent trap (such as molecular sieve) [13]. The performance or overall trapping efficiency (ξ_T) depends on the amount of C-11 released from the target, the amount of C-11 released from the trap and the time required for this process. The trapping efficiency ($\xi_{T'}$) is defined as the ratio of the amount of C-11 trapped to the amount of C-11 entering the trap, as shown in eq. 2.4 and indicates how well the trap retains the $^{11}\text{CO}_2$. The overall trapping efficiency is defined as the ratio of the amount of C-11 recovered from the trap to the amount of C-11 released from the target, as shown in eq. 2.5. The overall trapping efficiency can also be related to the trapping efficiency and the time required for trapping

and releasing the C-11, as shown in eq. 2.6.

$$\xi_{T'} = \frac{\text{C-11 trapped (mCi)}}{\text{C-11 entering trap (mCi)}} \quad (2.4)$$

$$\xi_T = \frac{\text{C-11 released from trap (mCi)}}{\text{C-11 released from target (mCi)}} \quad (2.5)$$

$$\xi_T = \xi_{T'} \cdot \exp^{-0.693 \cdot t_T/t_{1/2}} \quad (2.6)$$

Cryogenic $^{11}\text{CO}_2$ trap:

The trap typically consist of a small stainless steel tube, (40 cm x ϕ 0.02 mm). The tube is initially immersed in liquid nitrogen or liquid argon. The target gas is then flushed through the cold trap with an inert carrier gas such a helium, thus trapping the [^{11}C]carbon dioxide. The [^{11}C]carbon dioxide is recovered simply by passing a slow stream of inert carrier gas while heating the trap to room temperature. This requires removing the trap from the liquid nitrogen bath. Cryogenic $^{11}\text{CO}_2$ traps typically have a trapping efficiency of 90% using a stainless steel tube immersed in liquid nitrogen or argon with overall trapping/releasing time of approximately 5 minutes [13]. This corresponds to an overall trapping efficiency of 76%.

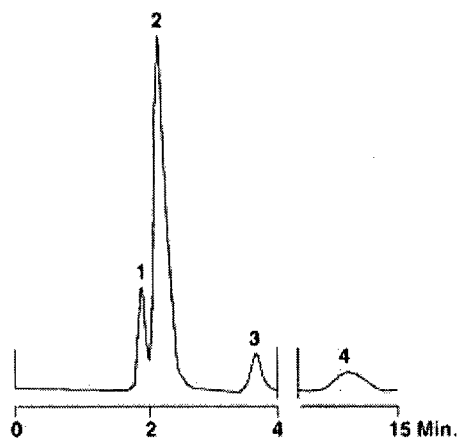
This method has been further improved, by the use of a stainless steel frit trap instead of a tube. The trap consist of a 2.25 cm long stainless steel check valve cartridge (for $\frac{1}{8}$ " tubing) which is packed with eight 20 μm stainless steel frits. The trapping efficiency was improved to 96% and overall trapping/releasing time was reduced to 3.9 minutes [35]. This corresponds to an overall trapping efficiency of 84%.

Molecular sieve $^{11}\text{CO}_2$ trap:

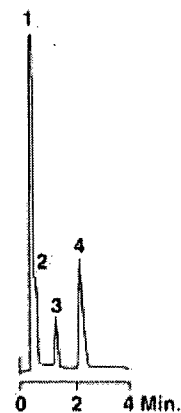
The basic principle behind the molecular sieve trap is chromatography. Chromatography is a method of separation that relies on differences in partitioning behavior between a flowing

mobile phase and a stationary phase to separate the components in a mixture. Molecular sieves have been used as packing for chromatographic recovery of $^{11}\text{CO}_2$ [13]. The trap typically consists of a column packed with zeolites molecular sieves. The target gas is unloaded through the trap, then flushed with inert gas, and heated to above 200°C for thermal desorption of the $^{11}\text{CO}_2$. For a column of the following dimensions, $l = 6\text{cm}$, $i.d. = 9\text{mm}$, packed with activated 60-80 mesh molecular sieve 4A, the trapping efficiency is above 98% [13]. With an overall trapping/releasing time of approximately 5 min, the trap releases 90% of the carbon dioxide when heated to 230°C . This corresponds to an overall trapping efficiency of 74%.

The tenacious affinities of zeolites for both CO_2 and water require careful activation before use and rather high thermal desorption temperatures. These inherent characteristics of zeolites lead to the development of an improved molecular sieve trap, with the use of carbon molecular sieves. In contrast to zeolites based materials, carbon sieves are quite hydrophobic in nature and have little affinity for water and small polar molecules. However, they avidly and selectively retain CO_2 then release it freely upon the application of modest heat. This is clearly illustrated when comparing the chromatograms of a carbon molecular sieve column at room temperature and at 140°C , as shown in Figure 2.1. A similar trapping procedure has been used, with a 65 cm long trap, 2 mm i.d., packed with 1 g of 80-100 mesh carbon molecular sieve. Trapping efficiency was essentially 100%, and 98% of the $^{11}\text{CO}_2$ was released from the trap heated to 100°C , with an overall trap/release time of 5 minutes [34]. This corresponds to an overall trapping efficiency of 83%. Control experiments showed that most of the carbon sieves tested did not significantly contribute $^{12}\text{CO}_2$ carrier to the final product [34].



A) 1. O₂, 2. N₂, 3. CO, 4. CH₄
20°C, 45 cm³/min He



B) 1. Air, 2. CO, 3. CH₄, 4. CO₂
140°C, 45 cm³/min N₂

Chromatogram, using carbon molecular sieve column, obtained from Alltech Inc. [36]

Figure 2.1: Separation of air, CO, CH₄ and CO₂ using gas chromatography

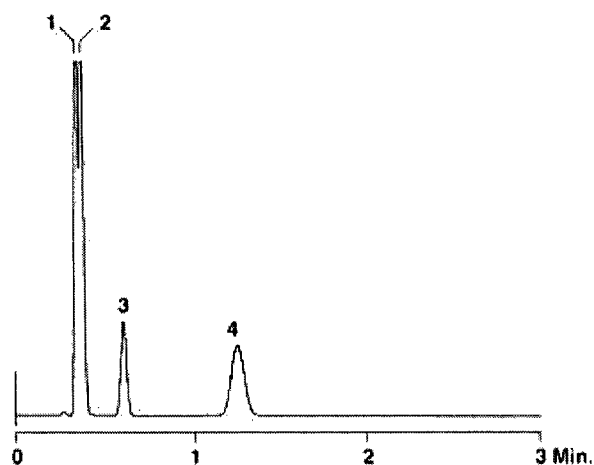
Cryogenic/chromatographic ¹¹CH₄ trap

In order to increase the retention time of ¹¹CH₄ in a chromatographic column and obtain separation from target gas, a combination of cryogenic trapping and chromatography are used. The trap consists of a tube packed with Poropak N (80-100 mesh). The trap is initially submerged in liquid nitrogen, after which the target is unloaded under controlled flow. As can be seen in Figure 2.2, heating to room temperature is sufficient to release the [¹¹C]methane. Trapping methane on Poropak N at -196°C is less efficient than trapping carbon dioxide on molecular sieves [22], with overall trapping releasing time approximately 6.0 minutes. Assuming that the trapping efficiency is 90%, this would correspond to an overall trapping efficiency of 73%.

2.1.3 Reduction of ¹¹CO₂ and oxidation of ¹¹CH₄

Reduction of ¹¹CO₂ to ¹¹CO

[¹¹C]Carbon monoxide was one of the first tracers used for blood flow measurement in humans [37]. Since it is less reactive than other [¹¹C]labeling agents, it has found little appli-



T = 35°C, 30 cm³/min He, 1. H₂, 2. Air, 3. CH₄, 4. CO₂
 Chromatogram, using poropak Q column, obtained from Alltech Inc. [36]

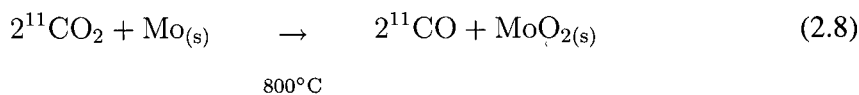
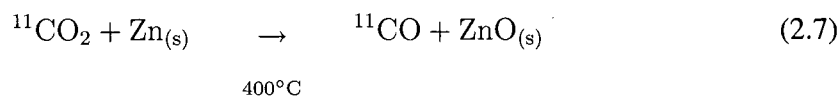
Figure 2.2: Separation of H₂, air, CH₄ and CO₂ using gas chromatography

cation as an intermediate in radiopharmaceutical syntheses. However, recently palladium catalyzed cross-coupling reactions for the direct preparation of ketones have been reported [38, 39]. [¹¹C]Carbon monoxide can be produced in situ or by reduction of [¹¹C]carbon dioxide on the surface of various transition metal elements.

An established method for [¹¹C]carbon monoxide preparation is the reaction of [¹¹C]carbon dioxide with zinc metal, as illustrated in eq. 2.7. Highest yields are obtained at 400°C which is very near the melting point of zinc (420°C), thus rigorous temperature control is required to avoid melting the zinc. The zinc granules must be thoroughly cleaned before use and require frequent replenishment. Yields are under 50% since a significant amount of radioactivity remains in the reactor [37].

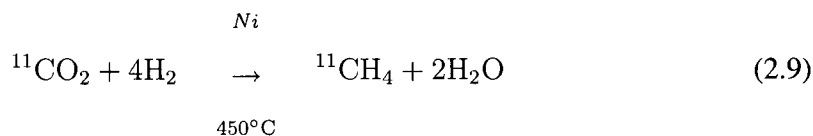
A more recent method for [¹¹C]carbon monoxide preparation is the reaction of [¹¹C]carbon dioxide with molybdenum metal (eq. 2.8). The reactor consisted of a 25 mm inner diameter quartz tube and 150 mm long, packed with 2000 m of 0.05 mm diameter molybdenum wire (99.97% Mo). A helium stream of 25 cm³/min (STP) was used to transfer the [¹¹C]carbon dioxide through the molybdenum reactor, which was kept at a preset temperature. Decay corrected yields of up to 81% were reported with reactor temperature of 800°C [40], with

a gas transfer and reaction time of approximately 3 minutes, resulting in a yield of 73%.



Reduction of $^{11}\text{CO}_2$ to $^{11}\text{CH}_4$

The reduction of $^{11}\text{CO}_2$ to $^{11}\text{CH}_4$ has been carried out for several applications, including preparation of [^{11}C]methyl iodide, [^{11}C]methyl triflate and [^{11}C]cyanide [2]. Although [^{11}C]methane can be produced in target, many PET centers choose to first produce [^{11}C]carbon dioxide and then react it with hydrogen using a nickel catalyst to produce [^{11}C]methane, as illustrated in eq. 2.9.



In gas chromatography, flame ionization detectors (FID) are not very sensitive to trace amounts of carbon oxides, but are much more sensitive to methane. Accordingly, nickel based catalyst are frequently used to convert trace amounts of carbon oxides to methane in order to improve the FID sensitivity.

In a unique setup, [^{11}C]carbon dioxide is reduced to [^{11}C]methane for production of [^{11}C]methyl triflate. The reactor consists of a nickel/alumina/silica (64% Ni) powder mixed with glass wool packed into a 4 mm inner diameter borosilicate glass tube. The purified

[^{11}C]carbon dioxide is swept from the trap with 10% hydrogen in nitrogen. The reactor oven is held at 450°C and the gas flowrate is approximately $50\text{ cm}^3/\text{min}$ (STP). Yields of [^{11}C]carbon dioxide to [^{11}C]methane routinely exceed 95% [41] in approximately 2 minutes, corresponding to a decay corrected yield of over 99%.

2.1.4 Synthesis of $^{11}\text{CH}_3\text{OH}$

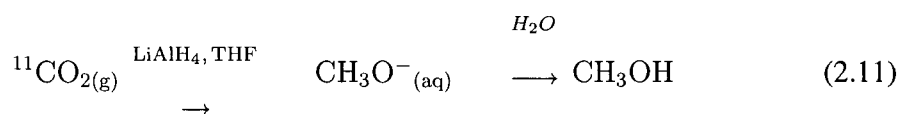
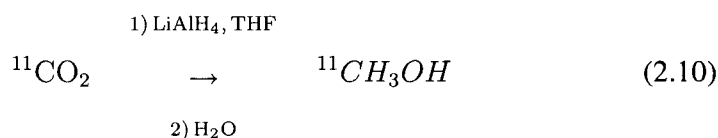
The established method to prepare [^{11}C]methanol involves the reduction of $^{11}\text{CO}_2$ to $^{11}\text{CH}_3\text{OH}$ using $\text{LiAlH}_4(\text{aq})$. This method produces low specific activity $^{11}\text{CH}_3\text{OH}$ due to contamination of LiAlH_4 with $^{12}\text{CO}_2$. To improve the specific activities of $^{11}\text{CH}_3\text{OH}$, alternate liquid phase and gas phase methanol synthesis routes have been investigated.

Liquid phase $^{11}\text{CH}_3\text{OH}$ synthesis

The conventional process for the reduction of [^{11}C]carbon dioxide to [^{11}C]methanol uses a solution of LiAlH_4 in tetrahydrofuran (THF), as shown in eq. 2.10. The $^{11}\text{CO}_2$ recovery from the trap is done with a gas stream of helium or nitrogen at flow rate of $10\text{-}100\text{ cm}^3/\text{min}$ (STP). The gas is dried over a dehydrating agent ($\text{MgClO}_4 \cdot \text{H}_2\text{O}$ or P_2O_5) and then the gas is bubbled through a solution of LiAlH_4 in THF. The solvent is then evaporated under a stream of nitrogen at approximately 100°C , leaving behind a dry radioactive complex from which [^{11}C]methanol is generated by the addition of water. The [^{11}C]methanol can be distilled for downstream use or alternatively hydroiodic acid can be added for in-vial preparation of [^{11}C]methyl iodide. An increase in the amount of LiAlH_4 leads to an increase in the yield, but a decrease in the specific activity. While a decrease in the amount of LiAlH_4 leads to an increase in the specific activity but a decrease in the yield. The preparation of methanol typically takes 3-4 minutes with decay corrected yield in the order of 75%, and corresponding yield of approximately 66% [1]. Reported specific activities for [^{11}C]methyl iodide produced via this procedure range from $0.1\text{-}1.7\text{ Ci}/\mu\text{mol}$ [1, 13].

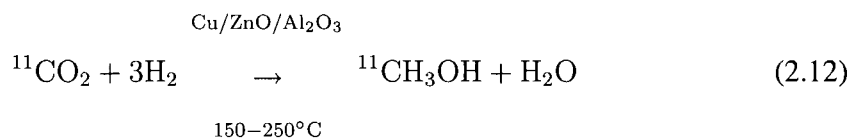
In attempts to reduce the amount of LiAlH_4 , a variation of the conventional method has

been developed, using LiAlH_4 adsorbed on alumina. The alumina cartridge is pretreated at 200°C under helium flow, for 1 hour, to desorb water and possible traces of carbon dioxide and then cooled to room temperature. It is then impregnated with $50\ \mu\text{l}$ of $1\ \text{M}$ LiAlH_4 diluted with $200\ \mu\text{l}$ diethyl ether. The $[^{11}\text{C}]$ carbon dioxide is trapped on the cartridge, after which it is heated up to 160°C under a $50\ \text{cm}^3/\text{min}$ flow of helium to remove the solvent. The dry complex is then hydrolyzed by injecting $0.01\ \text{M}$ phosphoric acid to form $[^{11}\text{C}]$ methanol. Decay corrected yields of 95% are reported with $[^{11}\text{C}]$ methanol preparation time of approximately 5 minutes, which corresponds to a yield of 80%. The specific activity of the downstream produced $[^{11}\text{C}]$ methyl iodide has been reported to be $2\text{-}2.5\ \text{Ci}/\mu\text{mol}$ [42, 13].



Gas phase $^{11}\text{CH}_3\text{OH}$ synthesis

Only a few publications report the catalytic conversion of $[^{11}\text{C}]$ carbon dioxide to $[^{11}\text{C}]$ methanol according to eq. 2.12.



J.T. Patt studied the synthesis of [^{11}C]methanol from [^{11}C]carbon oxides using Pd/Al₂O₃ and Cu/ZnO/Al₂O₃ catalysts [43]. Using either catalyst, and a mixture of ^{11}CO and/or $^{11}\text{CO}_2$, Ar, H₂ as feed gas, produced negligible amounts of methanol at 200-240°C and at 2-3 bar. The highest methanol yield obtained was 7%, with synthesis time of 25 min, at 240°C and at 2 bar, by adding N₂O to the feed stream [43].

A patent describes a pre-conditioning method of a catalyst prior to use for [^{11}C]methanol synthesis [44]. A copper-zinc oxide catalyst, supported on alumina and/or silica, is first reduced and then preconditioned with a stream of CO:CO₂:H₂ (1:1:8). Prior to [^{11}C]methanol synthesis, the catalyst is heated to 200°C and then gas containing [^{11}C]carbon dioxide and hydrogen is passed through the reactor at a pressure of 50 bar. The [^{11}C]methanol may remain adsorbed on the catalyst, and can be removed by addition of a catalyst poison, such as hydrogen sulphide or by increasing the temperature of the reactor to 280-320°C. The yield of [^{11}C]methanol is 57% and the specific activity ranging from 4-20 Ci/ μmol [44].

An alternative method uses $^{11}\text{CH}_4$ as starting material instead of $^{11}\text{CO}_2$. A mixture of $^{11}\text{CH}_4$, Cl₂ and H₂ is passed over Cr₂O₃ on pumice stone at 700°C in order to oxidize the $^{11}\text{CH}_4$ to $^{11}\text{CH}_3\text{OH}$ with yields up to 45% [45]. Synthesis time is 2 minutes decay corrected yield of 48%. The specific activity of the subsequently prepared $^{11}\text{CH}_3\text{I}$ was 1 Ci/ μmol [45].

2.1.5 Synthesis of carbon-11 radiopharmaceuticals

Most procedures to synthesize carbon-11 radiopharmaceuticals involve the methylation of an appropriate precursor. The reactivity of $^{11}\text{CH}_3\text{OH}$ is insufficient for most applications and accordingly the $^{11}\text{CH}_3\text{OH}$ needs to be converted to a more reactive intermediate, such as $^{11}\text{CH}_3\text{I}$. The preparation of [^{11}C]methyl iodide is done by reacting [^{11}C]methanol with a source of iodine, a step that does not affect the specific activity of the product.

Traditionally, [^{11}C]methyl iodide has been prepared by reaction of [^{11}C]methanol with hydrogen iodide under reflux [13]. The yield is above 90% [45, 42]. A more recent vari-

ation of this reaction route involves the use of aqueous HI impregnated on alumina, for which the yield was above 97% at optimal conditions [42]. Alternative iodination agents, diphosphorous tetra-iodide and triphenylphosphine diiodide, have been investigated for the production of [^{11}C]methyl iodide[46, 47]. The yields are similar as for the HI procedure, however by avoiding the use of volatile HI, the solid reagents allow a cleaner operation.

An alternative procedure, based on the iodination of [^{11}C]methane with iodine, has been pioneered by Larsen et al. [22, 21]. The reaction is carried out in a reactor in which [^{11}C]methane, helium and iodine vapors are mixed and heated. The formed [^{11}C]methyl iodide is continuously removed from the reactor while the unreacted [^{11}C]methane is recirculated through the reactor. The synthesis time is 10.5 minutes and reported yields are 58% with specific activity of 15 Ci/ μmol .

2.2 Molybdenum compounds for the reduction of CO_2 to CO

Molybdenum commonly occurs in nature as the mineral molybdenite, MoS_2 , in quartz rock. For this study molybdenum will be used to reduce carbon dioxide to carbon monoxide, by oxidizing the molybdenum. In this section, the history and chemistry of molybdenum, molybdenum oxides and molybdenum carbides are presented.

2.2.1 History

Molybdenum was discovered in 1778, but for the next hundred years, molybdenite was merely a laboratory curiosity. The first major use came during World War I when it was discovered that addition of molybdenum produced steels with excellent toughness and strength at high temperatures, suitable for use as tank armor and in aircraft engines [48].

Molybdenum is mainly used as an alloying element in steel, cast iron, and superalloys to increase hardenability, strength, toughness, and corrosion resistance. However,

it has found many other applications in lighting, electronics, vacuum coating and nuclear medicine. It is also extensively used as a catalyst or as a component thereof [48].

2.2.2 Reduction of molybdenum oxides

Reduction of molybdenum oxides with hydrogen

Molybdenum metal powder is produced industrially by reducing high-purity molybdenum compounds, such as molybdenum trioxide, ammonium hexamolybdate or ammonium dimolybdate, with hydrogen [48]. Molybdenum metal powder can be produced industrially by reducing MoO_3 powder with hydrogen between 500-1150°C [49]. Molybdenum trioxide, a gray-green powder is reduced by hydrogen at 500-600°C to MoO_2 , which is further reduced at 900-1050°C to molybdenum metal. Since the first reduction to MoO_2 is exothermic, this step is performed at 600°C to prevent caking due to the melting of MoO_3 (800°C). The red-brown MoO_2 [50] is reduced to metallic molybdenum powder at 1050°C. The powder has a particle size of 2-10 μm , a specific surface area of 0.1-1 m^2/g , and an oxygen content of 100-500 mg/kg (partly adsorbed and partly as oxide) [48].

Thermal decomposition and reduction of molybdenum trioxide under different reducing conditions has been extensively studied [51, 52, 53]. Molybdenum trioxide powder was reduced in pure hydrogen with gradual temperature increase from 300 to 800°C at approximately 6 °C/min and isothermally at 600°C. Under these conditions, the reduction of molybdenum trioxide to molybdenum dioxide took place at 387-615°C while the reduction to molybdenum metal took place slowly at 623-740°C[51].

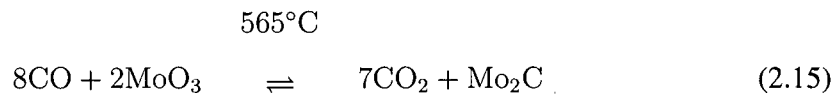
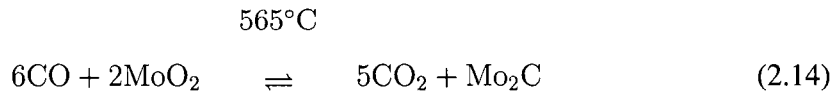
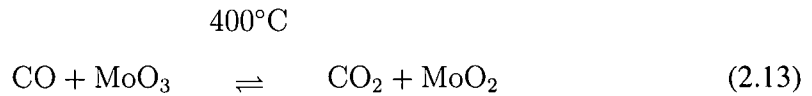
Lee et al. [54] performed temperature programmed reduction (TPR) of high purity molybdenum trioxide, from 300 to 750 °C, in pure hydrogen, with a heating rate of 1 °C/min. The gas products obtained during TPR were monitored by gas chromatography, equipped with thermal conductivity detector for the detection of water. Reduction of MoO_3 to MoO_2 occurred between 430-620°C, while complete reduction to molybdenum occurred above 700°C.

Iwasawa et al. [55] found that molybdenum dioxide on alumina was reduced with hydrogen to molybdenum at 600°C. In contrast to the one-step reduction mechanism of molybdenum trioxide to molybdenum dioxide, Burch [56] suggested that Mo_4O_{11} is an intermediate product of the reaction. However, Ressler et al. [53] found that Mo_4O_{11} was also formed by reaction of different molybdenum oxides. Temperature programmed reduction of MoO_3 with 5-100% H_2 was studied for temperatures ranging from 300-800°C. Between 350 and 425°C, the reduction of MoO_3 to MoO_2 is a one-step process without formation of crystalline intermediates. At temperatures above 450°C, Mo_4O_{11} can be obtained and its formation was explained as the product of a parallel reaction between molybdenum dioxide and molybdenum trioxide. There is a general agreement between various researchers that at reduction temperatures above 500°C and hydrogen concentrations of at least 10%, metallic molybdenum is produced as the final product according to a two step reduction, as illustrated in eqs. 4.2 and 4.3 [53].

Reduction of molybdenum oxides with carbon monoxide

Reduction of molybdenum trioxide with carbon monoxide at 400°C gave carbon dioxide, the reddish-brown molybdenum dioxide and unreacted molybdenum trioxide [57]. The reduction was presumed to proceed according to the eq. 2.13. At higher temperature (565°C), molybdenum trioxide in a stream of carbon monoxide gave carbon dioxide and a dark-gray almost black material, which was assumed to be molybdenum carbide and free carbon. The overall reaction is illustrated in eq. 2.15, which proceeds through intermediate eqs. 2.13 and 2.14. Further experiments were carried out with carbon dioxide (19%) and carbon monoxide (81%) and molybdenum dioxide at roughly 800°C, which yielded grayish molybdenum carbide, presumably according to the reversible eq. 2.14. The addition of carbon dioxide was to prevent build-up of carbon on the surface, which was confirmed by

the color and the carbon content of the molybdenum carbide [57].



Hexagonal Mo_2C is the only molybdenum-carbide phase of commercial interest and is the only phase that is stable below 1100°C [58]. It is produced as a powder in the micron range, with colors varying from white-gray to black [48, 59, 60]. It is stable in hydrogen, but it oxidizes in air above 500°C [48].

2.2.3 Oxidation of molybdenum

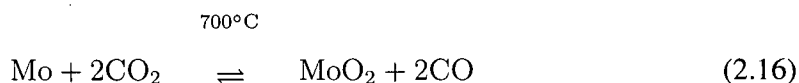
Oxidation of molybdenum with oxygen gas

Molybdenum retains its luster almost indefinitely in air, particularly when it has been drawn to fine wire. On prolonged heating in air below 600°C , the metal becomes covered with its trioxide; at 600°C the oxide sublimates and rapid oxidation occurs. Molybdenum burns in oxygen at $500\text{-}600^\circ\text{C}$ [48].

Oxidation of molybdenum with carbon dioxide

Vandenberghe reported that carbon dioxide reacts with molybdenum to form carbon monoxide and molybdenum trioxide above 700°C [61]. Spencer et al. [57] later pointed out that

these authors made no analysis of the solid product, but assumed that the molybdenum was oxidized to molybdenum trioxide. The progression of the oxidation was monitored by observations of the appearance of the solid phase. The colors suggested that the oxidation was carried only to the dioxide, according to eq. 2.16 [57, 61].

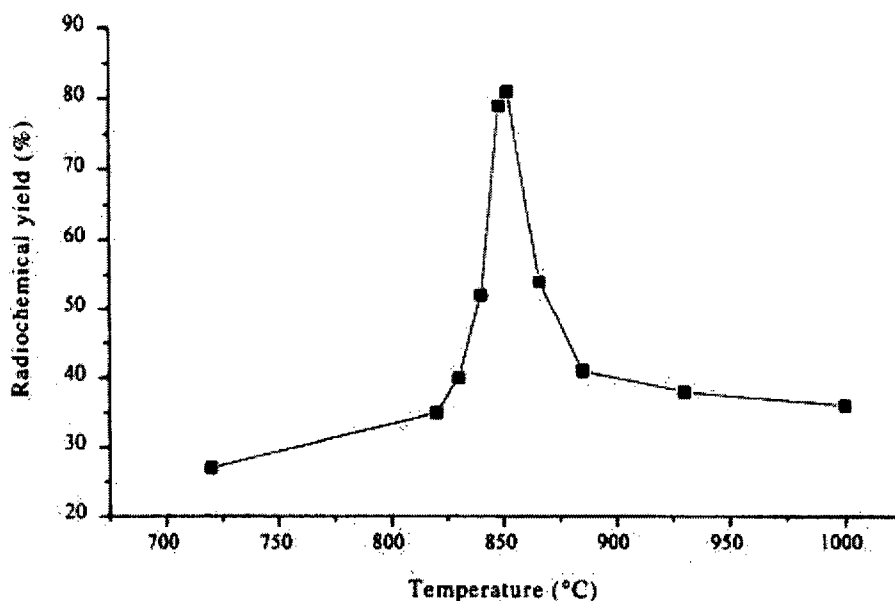


Hilpert et al. [62] indicated that at 1000°C, carbon monoxide passed over finely divided molybdenum leads to dimolybdenum carbide. At 800°C they obtained a carbide of high carbon content by reacting carbon monoxide with molybdenum trioxide. Smith et al. [63] previously observed no reaction when molybdenum was heated to a over 1000°C in an atmosphere of carbon monoxide. Lian et al. [64] demonstrated that at room temperature and at 80°C, H₂, N₂, CH₄ and CO showed no reactivity with molybdenum atoms, while O₂ and CO₂ both reacted with molybdenum.

Thin molybdenum wire is reported to react with ¹¹CO₂ between 700 and 1000°C for the formation of ¹¹CO, and it was concluded to proceed according to eq. 2.8. Chemical conversions of up to to 80% were reported, over a narrow temperature range, 840-860°C, as illustrated in figure 2.3. At 825°C ¹¹CO₂ decay corrected yield was 35% and decreased with decreasing temperature, while at 875°C, ¹¹CO₂ decay corrected yield was 45% and decreased with increasing temperature.

2.2.4 Interaction of CO₂ and CO with Mo₂C

Mo₂C is used in special cemented carbide grades containing TiC and nickel metal. Most Mo₂C is used in steel alloys, where it forms during melting. Although MoO₃ or MoO₂ can be carburized with carbon at 1500°C, a carbide with the correct carbon content and a



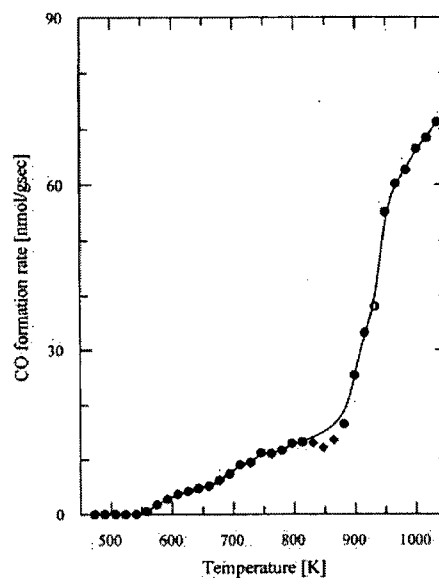
Radiochemical yield, i.e. decay corrected to EOB, from Zeilser et al. [40]

Figure 2.3: Decay corrected ^{11}CO yields as a function of temperature

low oxygen content is difficult to obtain. Pure Mo_2C is best made by heating molybdenum metal powder with carbon in hydrogen at 1500°C [65].

Molybdenum carbide is also used extensively as a catalyst, such as for aromatization of ethane, ethylene, propane and in the oxidative dehydrogenation of these compounds using carbon dioxide as an oxidant. The catalyst is prepared by heating molybdenum trioxide in a stream of methane and hydrogen, from 500 to 800°C [54]. During preparation, surface contamination by carbon generally occurs. The latter can be removed by treatment with hydrogen under controlled environment. Once the excess carbon was completely removed, it was observed that the BET surface area of the catalyst and CO chemisorption were highest. For a catalyst treated with hydrogen, the surface area was found to be $60\text{ m}^2/\text{g}$, with a CO uptake at room temperature of $220\text{ }\mu\text{mol}/\text{g}$ [54].

Lee et al. [54] showed that the molybdenum metal has a much lower surface area than the Mo_2C catalyst. The Mo_2C had a BET surface area of $60\text{-}100\text{ m}^2/\text{g}$ while TPR of MoO_3 with hydrogen yielded molybdenum with BET surface area of $3\text{ m}^2/\text{g}$. Prior



From Solymosi et al. [66]

Figure 2.4: CO formation rate from temperature programmed reaction of CO_2 with Mo_2C to removal from the reactor, the dimolybdenum carbide was passivated with 1% oxygen at room temperature [54]. Molybdenum can be passivated by oxidation, especially by electrolytic oxidation, becoming chemically unreactive [48]. Iwasawa et al. [55] observed deposition of small amounts of carbon on molybdenum fixed on alumina, after it had been reduced with hydrogen at 500°C for 5 h.

Solymosi et al. [66] studied the reaction between carbon dioxide and supported Mo_2C . Temperature programmed reaction of carbon dioxide with supported Mo_2C forms carbon monoxide, as illustrated in figure 2.4. Carbon monoxide was first detected at 300°C , and a more extensive decomposition of carbon dioxide to carbon monoxide occurred above 600°C [66]. Using $^{13}\text{CO}_2$ as supply gas, it was demonstrated that over 90% of the CO was formed from the supply gas and not from the carbide [66]. It was demonstrated that the CO comes mainly from decomposition of CO_2 , according to eq. 2.17, and that the contribution of the reaction of carbon in Mo_2C with the O atom formed in the CO_2 dissociation, according to eq. 2.18, is limited [66].



The reaction between 25% CO_2 and Mo_2C was carried out for several hours at 800°C and complete oxidation to MoO_3 did not occur [66].

2.3 Methanol synthesis

2.3.1 History

The history of industrial methanol synthesis covers over three quarters of a century, with the first barrel of synthetic methanol produced at BASF, Germany, in 1923. The first industrial methanol synthesis process is known as the high pressure process, which operated at 250-300 bar and $320\text{-}450^\circ\text{C}$, and was the dominant technology for 45 years. The feed syngas was based on coal/lignite, which generally contained a significant amount of poisons, such as chlorine and sulfur. Accordingly, a relatively poison-resistant catalyst was developed, based on zinc oxide / chromium oxide. However, further developments found that copper increased the selectivity to methanol, and that zinc was an efficient dispersant of copper [67]. The copper based catalyst is quite easily deactivated by poisons found in coal/lignite, though this problem was overcome by utilizing synthetic gas originating from natural gas and removal of catalyst poisons prior to methanol synthesis. Accordingly, a low pressure process was developed in the late 1960's, which operates at much milder conditions, i.e. 35-55 bar and $200\text{-}300^\circ\text{C}$. The low pressure process is still the dominant process being used today [68].

2.3.2 Catalyst preparation

Many different types of catalysts have been studied, including co-precipitated copper-zinc oxide, co-precipitated copper-zinc oxide alumina, Raney copper, intermetallic compounds and precious metals such as palladium [69]. The current catalysts used in industrial low pressure methanol synthesis are based on copper / zinc oxide / alumina with possible additives such as magnesium oxide [67]. The ratios of components vary from one manufacturer to another, but typically the copper oxide ranges between 25-80%, zinc oxide between 10-50% and the alumina between 5-10% [68]. Commercially available low pressure methanol catalysts have a methanol selectivity above 99% [68].

The low pressure catalysts are obtained as metal hydroxycarbonates or nitrates by co-precipitation of a multi-metal nitrate solution with a solution of sodium carbonate [70, 71]. Preparation parameters, such as pH, temperature, composition, duration, play an important role in the quality of the produced catalyst. A typical sequence for co-precipitation is the following:

1. Prepare solution of zinc, copper and aluminum nitrates to desired ratio
2. Co-precipitate metal ions using a solution of sodium carbonate
3. Filter metal carbonates and wash with water
4. Dry metal carbonates at 120°C
5. Calcinate the metal carbonates in air at 300-500°C
6. Pelletize metal oxides
7. Activate the resulting catalyst by reduction in 2% hydrogen at 250°C

Prior to reduction, the commercial catalysts have a BET surface area of 60-100 m²/g, which is reduced to 20-30 m²/g after reduction [68].

Activation of freshly prepared industrial catalyst is generally carried out by reduction in a 1-5% H₂/N₂ at 1 bar for several hours by ramping up the temperature to 240°C (~30 °C/h) and holding at this temperature for several hours. The reduction of CuO/ZnO and CuO/ZnO/Al₂O₃ catalysts, with 2% hydrogen in nitrogen at 250°C and 1 bar has been demonstrated to reduce the CuO to Cu metal, via the intermediate Cu₂O [70]. At these conditions, the copper oxide is fully reduced to copper metal, without any residual copper oxide remaining [67].

2.3.3 Catalyst poisoning / deactivation

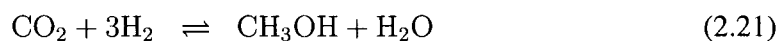
Halogen compounds are known to poison the copper surface, so methanol feed gas needs to be halogen free [69]. Other impurities in the catalyst itself, such as silicon compounds, nickel carbonyls or iron carbonyls, can cause damage to the catalyst [68]. The catalyst can also be deactivated when the reactor is operated in the absence of oxidizing agent such as carbon dioxide [70]. Experiments using a mixture consisting of only H₂/CO rapidly and irreversibly deactivated the catalyst [71]. Methanol yields have been enhanced by the presence of carbon dioxide, water, and/or oxygen [72]. Experiments performed by pulsing oxygen to a CO/H₂ feed indicated that up to a 15 fold increase of methanol yields could be obtained [72]. Active sites for methanol synthesis can be deactivated when the catalyst is operated for extended periods of time at elevated temperatures above 245°C [72, 69].

2.3.4 Thermodynamics and kinetics

Methanol synthesis, typically involves five components: hydrogen, carbon dioxide, carbon monoxide, water and the product methanol. The role of carbon dioxide in the reaction mechanism has been an ongoing debate [73].

Until the early 1980's, mechanistic considerations were based mainly on the reaction between carbon monoxide and hydrogen, illustrated in eq. 2.19 [68]. The higher yields achieved by the addition of carbon dioxide was attributed to the displacement of the re-

verse water gas shift equilibrium 2.20. In addition, carbon dioxide was believed to affect the oxidation state of the active sites in the catalyst [70]. Alternatively, it was proposed that methanol was formed uniquely due to the reaction of hydrogen and carbon dioxide, illustrated in eq. 2.21 [74]. Recent experiments with isotope labelled reactants showed that both reactions 2.19 and 2.21 are possible [68].



Reaction enthalpies can be determined from the standard enthalpies of the reactants and products, and are -91 kJ/mol for eq. 2.19, -49 kJ/mol for eq. 2.21. Both reactions for methanol synthesis are exothermic and consequently methanol synthesis is favored by low temperature and high pressure. Additionally, the reaction of carbon dioxide with hydrogen, known as the reverse water-gas shift reaction, shown in eq. 2.20, must be taken into account. The enthalpy for the reverse water-gas shift reaction, is 41 kJ/mol. Consequently, this endothermic reaction is favored by high temperatures and low pressure.

Chapter 3

Experimental: Trapping and purification of $^{11}\text{CO}_2$

The key intermediate in the radiosynthesis of many carbon-11 radiopharmaceuticals is $[^{11}\text{C}]$ methanol. This study focuses on the feasibility of a gas phase methanol synthesis, the optimization of the main steps involved and its applicability to the radiosynthesis of $[^{11}\text{C}]$ methanol. The three principal steps evaluated in this study include:

1. Trapping and purification of $[^{11}\text{C}]$ carbon dioxide
2. Conversion of carbon dioxide to carbon monoxide using molybdenum
3. Methanol synthesis from carbon monoxide and hydrogen over a copper zinc oxide catalyst

3.1 Introduction

The $^{11}\text{CO}_2$ is produced in a cyclotron and subsequently concentrated in a carbon molecular sieve trap. The effect of temperature and mass of carbon molecular sieves on the trap performance was examined by computing the trapping efficiency, illustrated in eq. 2.4. The

overall trapping efficiency, illustrated in eq. 2.6, is based on the irradiation conditions for production of carbon-11 (proton current, proton energy, irradiation time) and on trapping data (amount $^{11}\text{CO}_2$ not trapped, amount of $^{11}\text{CO}_2$ released from trap and time required).

3.2 Materials and methods

Irradiations were performed with the Ebco Technologies TR19 cyclotron of the CHUS PET facilities, Sherbrooke, QC. Capintec dose calibrators were used for quantitative measurement of carbon-11. The target used is an Ebco Technologies gas target, consisting of a water-cooled aluminum cylindrical body, which contains the target gas. Two Havar windows, which separate the high pressure gas target from the high vacuum cyclotron, are cooled with helium.

A trap was designed such that it could be cooled to -20°C and rapidly heated to 110°C . The prototype trap was built at Ebco Technologies. Thermo-electric coolers (TEC's) were selected for their ability to be remotely controlled by computer and their relatively rapid cooling time. They have the advantage over conventional cryogenic traps that no liquid nitrogen is required and thus no moving parts are necessary. The TEC's require a DC voltage input, therefore the trap cooling can be remotely controlled by computer. This increases the level of automation in the final synthesis module and enables repeated productions without having to access the unit. To provide fast heating, a 325 W cartridge heater were used, combined with the TEC's operated in reverse mode, which provided an additional 100 W heating power.

The final trap design implemented consisted of a copper block, through which a U shape was machined and onto which two 35 mm long 6.35 mm outer diameter copper tubes were brazed. The U shape trap was then packed with carbon molecular sieve (Carbosphere 60-80 mesh) and both ends were plugged with quartz wool. Additionally, a 6.35 mm diameter hole was bored through the copper block, in which the 325 W cartridge heater was placed.

A K-type thermocouple was mounted on the copper trap to monitor temperature and allow temperature control. The copper block was screwed onto an aluminum heat sink block, with 2 thermo-electric coolers (TEC's) placed in between. A hole was drilled through the aluminum block and connected to a supply of cooling water, to remove the heat generated by the TEC's during the cooling step. After trap assembly, the carbospheres were conditioned by heating to 250°C and under flow of helium for 2 hours. Nitrogen/oxygen (UHP 99.5% N₂, 0.5% O₂) for the production of carbon-11 and helium (Helium UHP) were available on site at the CHUS facilities.

The temperature was controlled by a manual thermostat, obtained from Omega. The flow rate of the helium sweep gas was controlled by a mass flow controller, obtained from MKS. The mass flow controller was calibrated using the soap bubble method, for which calibration curves are illustrated on page 91. Solenoid valves, 2-way normally closed, were obtained from Precision Dynamics. A check valve, with cracking pressure of 0.3 bar, was obtained from Swagelok. A control panel, to enable remote control of valves, reactor temperature and mass flow controller was built by Ebco Technologies.

3.3 Experimental set-up

Figure 3.1 illustrates the experimental setup used to determine the trapping efficiencies. The [¹¹C]carbon dioxide trap, the solenoid valve for helium gas supply, the mass flow control valve for helium flow control, the check valve and Ascarite column were located in a lead shielded hot cell. The cyclotron was located in a concrete shielded vault. The target was installed on the cyclotron target selector, which is locally shielded.

3.4 Experimental procedure

The trapping efficiencies of a copper tubular trap, with 4 different amounts of carbon molecular sieves, were measured with the experimental configuration illustrated in figure 3.1, for

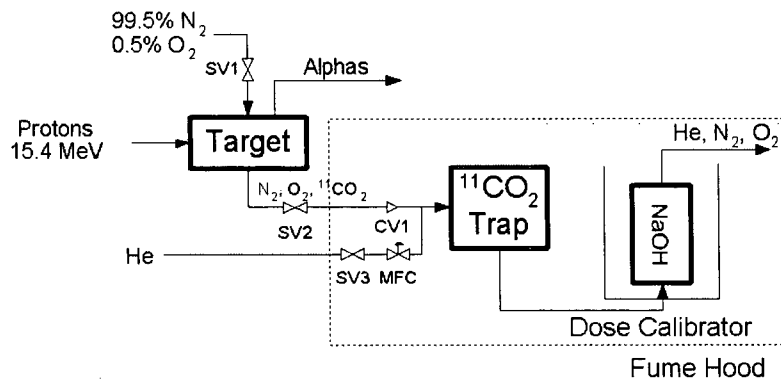


Figure 3.1: $^{11}\text{CO}_2$ Trapping experimental flow diagram

temperatures varying from -20°C to 100°C . The experimental procedure can be separated into two distinct major steps; production of $^{11}\text{CO}_2$ and $^{11}\text{CO}_2$ trapping, purification and release.

3.4.1 Production of $^{11}\text{CO}_2$

$[^{11}\text{C}]$ Carbon dioxide was produced by proton irradiation of the nitrogen/oxygen filled gas target. The gas target and all valves to control the filling/unloading were already in place at the CHUS PET facilities. Thus the target loading and unloading were done using the current setup implemented at CHUS for $[^{11}\text{C}]$ acetate production, with the unload line re-plumbed to connect it to the experimental setup located in the hot cell.

The 22 cm^3 (STP) target was filled to 17 bar. Once the cyclotron was in operation at a few μA , the target was positioned so that at least 80% of the beam bombarded the target. The current was then increased to approximately $10\ \mu\text{A}$, while monitoring the target pressure, ensuring that it did not exceed 25 bar. A saturated yield of C-11 is produced in roughly 40 min of bombardment. However, for these tests, only small amounts of radioactivity were desired, mainly to keep exposure to radiation below allowable levels set by Health Canada. Consequently 10 min of bombardment was sufficient. The cyclotron energy was not modified, and remained at the preset value of 15.4 MeV. Due to energy drop across the Havar foils, the beam energy that actually irradiates the target gas was about

14 MeV.

Several control runs were performed in order to determine the yield of the target. The target was irradiated as above, and its contents were directly emptied in an Ascarite trap located in the Capintec dose calibrator. This allows measurement of total amount of [11]CO₂ produced in target as a function of irradiation conditions, namely beam intensity and irradiation duration. Ten control runs were performed and the target yield was determined using eq. 2.3. For subsequent experiments, the amount of 11 CO₂ produced in target was computed based on the target yield, proton beam intensity and an irradiation duration, using eq. 2.3.

The steps involved in the production of 11 CO₂ are the following:

1. Turn on cyclotron (Ion source, main magnet, vacuum, utilities, target window cooling, target cooling, RF)
2. Open the main valve on the nitrogen/oxygen gas cylinder
3. Set the pressure regulator to read 17 bar
4. Open the target valve
5. Close the target valve once pressure sensor read-back is roughly 17 bar
6. Set the N₂/ O₂ pressure regulator to 8 bar(for target rinse)
7. Remove ion beam stop (IBS) (now beam will be on target)
8. Adjust cyclotron main magnet
9. Adjust position of target
10. Increase proton beam to 10 μ A
11. Irradiate for 10 min

3.4.2 Trapping and release of $^{11}\text{CO}_2$

Prior to production of the $^{11}\text{CO}_2$, the trap water cooling valve was opened and the TEC's were turned on. A stable trap temperature of -20°C was reached in less than 10 min. The target gas was unloaded through the pre-cooled trap and rinsed with 8 bar N_2/O_2 mixture. The trap was then rinsed with UHP He at flow-rates up to 70 cm^3 (STP). The trap was closed and heated to 110°C . The $^{11}\text{CO}_2$ was released with a stream of He and then trapped in a sodium hydroxide column. The sodium hydroxide column was placed in a dose calibrator, to allow continuous measurement of $^{11}\text{CO}_2$. This enabled quantification of the amount of $^{11}\text{CO}_2$ not trapped by the trap, and also the amount released from the trap. These quantities were decay corrected to end of the bombardment (EOB) (eq. 2.2), to enable determination of the overall trapping efficiency (eq. 2.5). In order to ensure that no activity remains on the trap, it was disassembled and placed in the dose calibrator.

The steps involved in the $^{11}\text{CO}_2$ trapping and releasing are the following:

1. Turn on cooling water and TEC
2. Open valve on helium gas cylinder and set regulator to 2 bar
3. Set mass flow-control valve to desired set point
4. Place a fresh sodium hydroxide column in dose calibrator
5. Open valve to unload target
6. Make sure target pressure is below 8 bar
7. Open valves on carbon molecular sieve trap
8. Measure amount of $^{11}\text{CO}_2$ breakthrough throughout unloading step
9. Close valve to unload target
10. Open valve to fill target with N_2/O_2 to rinse target and close after 10 s

11. Open valve to unload target
12. When the target pressure is ~ atmospheric, close all valves
13. Open Helium supply valve to rinse trap for 30 s
14. Heat trap (until release temperature is reached)
15. Flush helium through cold trap
16. Note radioactivity reading every 15 s

3.5 Results and discussion

The target yield was determined to be 83 ± 4 mCi/ μ A, for an extracted beam energy of 15.4 MeV and energy on target of approximately 14 MeV. As can be seen in table 3.1, this value is lower than other reported experimental and theoretical yields. The target was subsequently redesigned to give a yield of about 150 mCi/ μ A.

Table 3.1: C-11 target yields, 14 MeV

Target	Yield (mCi/ μ A)
Ebco improved target	150
Ebco target	83 ± 4
Vandewalle et al.[32]	135 ± 7
Casella et al.[30]	92
Theoretical yield[31]	169

The time required for each step of the trapping sequence was determined in a systematic fashion. The unload time was set to 30 s since at that time the pressure in the target had dropped to nearly atmospheric. The time required for the rinse target step was set to 15 s, corresponding to the time required to manually perform the sequence of valve actuation. The time for the second target unload was determined by monitoring the radioactivity collected in an Ascarite column, with the $^{11}\text{CO}_2$ trap bypassed. A maximum value was seen after 45 s. Additional runs were done with 2 target rinses, however no significant amount

Table 3.2: $^{11}\text{CO}_2$ trapping/releasing Sequence

Step	Description	Time elapsed (min:s)
1	Unload target (EOB)	0:00
2	Rinse target	0:30
3	Unload target	0:45
4	He Rinse trap	1:30
5	Heat trap	2:00
6	Release $^{11}\text{CO}_2$	2:30

Table 3.3: $^{11}\text{CO}_2$ trapping efficiencies

Trap	Carbosphere (g)	Trapping efficiency (\pm STDEV)
1	1.0	25% \pm 2% (n=4)
2	1.3	45% \pm 2% (n=4)
3	1.9	92% \pm 1% (n=4)
4	2.8	99% \pm 1% (n=4)

of additional C-11 was recovered. The He rinse of the trap was set to 30 s, to allow sufficient time to remove the target gas from the trap [34]. The time for heating the trap to 110°C was 30 s. Table 3.2 illustrates the final sequence used, with the time (from EOB) at which each step was executed.

3.5.1 Effect of carbon molecular sieve mass on $^{11}\text{CO}_2$ trapping efficiency

The amount of carbon molecular sieves necessary for optimal trapping was determined by comparing the trapping efficiencies for different amounts of carbon molecular sieves. The pre-cooled trap temperature was typically -20°C and the amount of 60-100 mesh carbon molecular sieves, was varied from 1.2 g to 2.8 g. Table 3.3 illustrates the trapping efficiencies for four different amounts of carbon molecular sieve.

As the amount of carbon molecular sieves increases, the trapping efficiency increases. However, with increasing amount of carbon molecular sieves, the time required for $^{11}\text{CO}_2$ recovery will likely increase and the volume in which the $^{11}\text{CO}_2$ is delivered to downstream process may be larger. Thus the amount of carbon molecular sieves used for subsequent

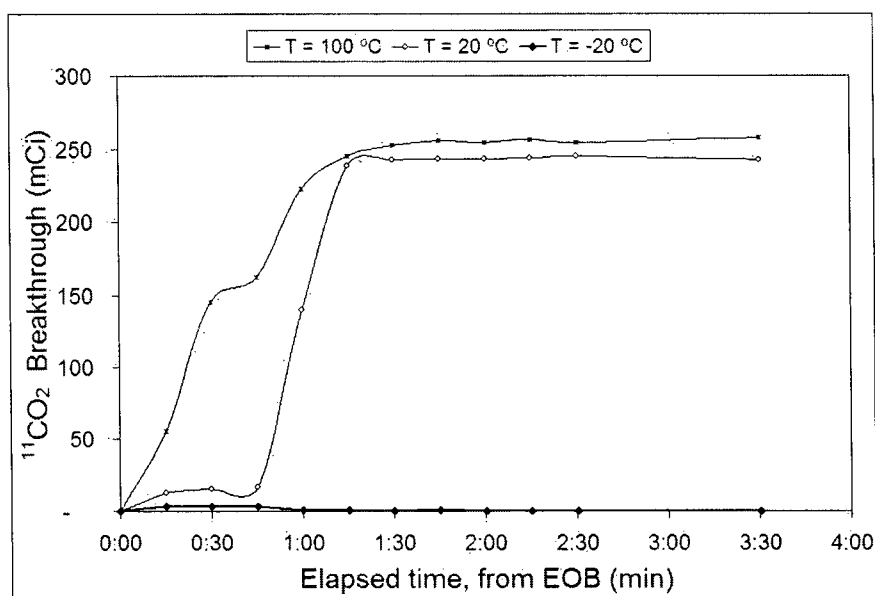


Figure 3.2: $^{11}\text{CO}_2$ activity vs. time, for different trap temperatures.

experiments was set to 2.0 g, i.e. the lowest amount required to obtain above 95% trapping efficiencies. The optimal amount will vary with target volume, target pressure, length and size of tubing from the target to the trap and trapping temperature.

3.5.2 Effect of trap temperature on CO_2 trapping efficiency

The temperature required for optimal trapping was determined by comparing the trapping characteristics at different trapping temperatures. The trap temperature was kept constant for each run, and the sequence shown in table 3.2 was used, with steps 5 and 6 omitted. Thus, the He rinse step was continued until 10 minutes EOB. Figure 3.2 illustrates the effect of temperature on the retention of $^{11}\text{CO}_2$ in the trap. At 100°C , the trap did not retain any significant amount of $^{11}\text{CO}_2$. At room temperature, there was a slight delay before the activity was seen in the ascarite column. At -20°C , the activity remains on the trap even after 10 minutes EOB. The initial amount of $^{11}\text{CO}_2$ at EOB was approximately 250 mCi in each case.

Table 3.4: Comparison of overall trapping efficiency

Trap	Overall trapping efficiency
Cryogenic [13, 35]	76-84%
Molecular sieve 13x[13]	74%
Carbon molecular sieve[34]	83%
Carbon molecular sieve (this work)	88% ±2%

3.5.3 Overall trapping efficiency

For a trapping efficiency of 99% obtained using 2.8 g carbon molecular sieve at -20°C, the time required to deliver the $^{11}\text{CO}_2$ was 3.5 minutes. This corresponds to an overall trapping efficiency of 88%, which is competitive with reported results (see table 3.4). This would be sufficient for incorporating into a system for routine production of carbon-11 radiopharmaceuticals.

Chapter 4

Experimental: Reduction of CO_2 to CO

4.1 Introduction

The following step in the overall process for $^{11}\text{CH}_3\text{OH}$ preparation is the reduction of $^{11}\text{CO}_2$ to ^{11}CO . Yields up to 80% were reported at 850°C for the reduction of $^{11}\text{CO}_2$ to ^{11}CO using molybdenum [1], as described in section 2.1.3. No special treatment to the molybdenum was done prior to reaction, and the reaction proceeds by direct oxidation of molybdenum to molybdenum dioxide as shown in eq. 2.8 [75].

4.2 Preliminary experiments: reaction of $^{11}\text{CO}_2$ and Mo

Preliminary experiments for the reduction of carbon dioxide were performed at the CHUS PET facilities, Sherbrooke, QC, using $^{11}\text{CO}_2$.

4.2.1 Materials and methods

The $^{11}\text{CO}_2$ was produced and purified using procedure described in Chapter 3 on page 34. The carbon dioxide/carbon monoxide reactor consisted of a 9.5 mm outer diameter cylindrical quartz tube with 6 mm inner diameter, packed uniformly with 2.3 g of molybdenum

wire, 0.05 mm diameter and 500 m (Goodfellow Corp). The quartz tube was horizontally mounted in a 400 W ceramic tubular heater (Omega). The temperature was measured with a K-type thermocouple (Omega) and controlled with a manual thermostat (Omega).

A mass flow controller, obtained from MKS, was used to control the flow rate of the helium sweep gas. It was calibrated by varying the input voltage from 0-5 V, and the output flow of helium was measured using the soap-bubble technique. The flowrates were corrected to STP using the ideal gas law. The resulting calibration curve is illustrated on page 92. Solenoid valves, 2-way normally closed, were obtained from Precision Dynamics. A control panel, to enable remote control operation of valves, reactor temperature and mass flow controller, was built by Ebco.

4.2.2 Experimental set-up

The flow diagram for the experiments using $^{11}\text{CO}_2$ is illustrated in figure 4.1. The same set-up was used as described in section 3.3 for production and release of $^{11}\text{CO}_2$. The molybdenum reactor was added to the outlet of the $^{11}\text{CO}_2$ trap, followed by an Ascarite (Aldrich) trap and a silica (Aldrich) trap, which was cooled with liquid nitrogen. At the outlet of the reactor, a solenoid valve was placed to avoid exposure to atmosphere. The setup was located in a lead shielded hot cell, with all valves / flowmeter controlled remotely.

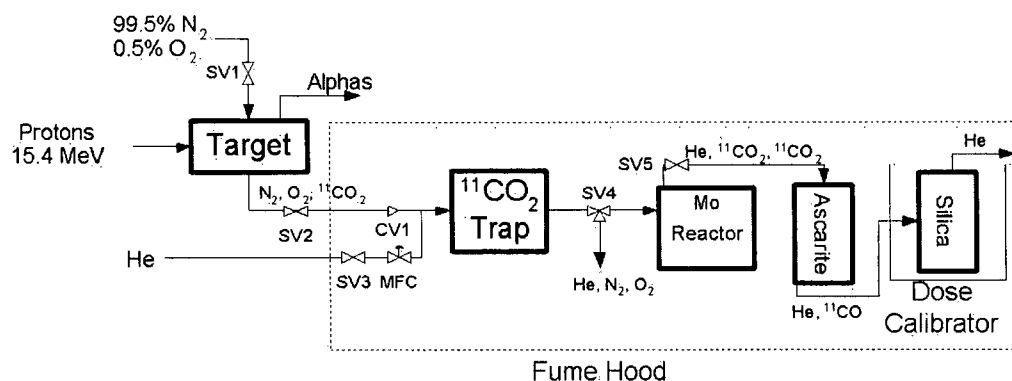


Figure 4.1: $^{11}\text{CO}_2$ Reduction experimental flow diagram

4.2.3 Experimental procedure

The production of $^{11}\text{CO}_2$ was carried out as in the $^{11}\text{CO}_2$ trapping experiments, described in section 3.4.1. The irradiation condition were noted to enable quantification of the total amount of $^{11}\text{CO}_2$ produced in target. The $^{11}\text{CO}_2$ trap was conditioned by flowing helium at 250°C for 2 h. Initial experiments were carried out with molybdenum as-supplied. Subsequently, experiments were carried out after pre-reducing the molybdenum with 10 % hydrogen in helium at 850°C . The silica gel trap was initially conditioned by heating to 650°C while purging with helium. The molybdenum oven was preheated to 800, 850, 900 and 950°C , under flow of helium. The $^{11}\text{CO}_2$ was released from the $^{11}\text{CO}_2$ trap at 17.5, 35 and $70\text{ cm}^3/\text{min}$ (STP) helium, through the molybdenum reactor, the Ascarite column and the silica column submerged in liquid nitrogen. The cold silica column was placed in the dose calibrator to measure the amount of ^{11}CO . When the activity on the silica column reached a maximum, the amount of $^{11}\text{CO}_2$ on the Ascarite was likewise measured by placing the column in the dose calibrator. This enabled quantification of the amount of unreacted $^{11}\text{CO}_2$ that had been released from the reactor. To minimize exposure to radiation, long thongs were used to place the Ascarite trap in the dose calibrator. The decay corrected conversion of $^{11}\text{CO}_2$ to ^{11}CO was computed based on the amount of activity produced in target and the amount of ^{11}CO measured. Table 4.1 illustrates the sequence that was used, with the time from EOB at which each step was executed.

4.2.4 Results and discussion

Initial experiments resulted in $^{11}\text{CO}_2$ conversion to ^{11}CO of about 5%. At the end of the experiments, it was observed that the molybdenum surface was no longer a shiny metallic color but a dull grayish color. Since the industrial compound MoO_3 is described as a gray-green powder [48], it was suspected that the molybdenum was oxidized. Molybdenum metal powder is produced industrially by reducing compounds such as MoO_3 powder with

Table 4.1: $^{11}\text{CO}_2$ Reduction sequence

Step	Description	Time elapsed (min:s)
1	Unload target (EOB)	0:00
2	Rinse target	0:30
3	Unload target	0:45
4	He rinse trap	1:30
5	Heat trap	2:00
6	Release $^{11}\text{CO}_2$	2:30
7	^{11}CO measurement	6:30
8	$^{11}\text{CO}_2$ measurement	7:30

Table 4.2: Summary of ^{11}CO yields, 17.5-70 cm^3/min , 2 bar

T ($^\circ\text{C}$)	Yield (decay corrected)	S.D.
800	6%	2%
850	8%	2%
900	9%	4%
950	8%	2%

hydrogen between 500-1150 $^\circ\text{C}$ [49]. In order to reduce the molybdenum trioxide back to the metallic state, 10% hydrogen in argon was flowed through the reactor at 850 $^\circ\text{C}$, for 30 min. Thereafter, experiments were resumed. Decay corrected yields were calculated based on eq. 2.2. The amount of [^{11}C]carbon dioxide produced in the target at the end of bombardment was computed using eq. 2.3, based on the target yield (see table 3.1), beam current and irradiation duration. A summary of the decay corrected yields obtained during hot experiments are given in table 4.2. For each temperature tested, at helium flow rates of 17.5, 35 and 70 cm^3/min (STP), the average conversion of $^{11}\text{CO}_2$ to ^{11}CO was at most 9%. Based on these results, there is no apparent correlation between flow and/or temperature with conversion. Conversion in the order of 80% was expected based on published data [40].

After completing the hot experiments, the molybdenum was again a dull grayish color indicating that oxidation may have occurred. It is suspected that the helium flush of the $^{11}\text{CO}_2$ trap was insufficient, and that some of the oxygen from the target gas remained in the $^{11}\text{CO}_2$ trap. When attempting to reduce the $^{11}\text{CO}_2$ with the molybdenum reactor, the

residual oxygen may have oxidized the molybdenum. Molybdenum retains its luster almost indefinitely in air, particularly when it has been drawn to fine wire. However, when heated in air, oxidation occurs and renders the surface chemically unreactive [48]. Consequently, for future use it is recommended to ensure that all oxygen is removed from the $^{11}\text{CO}_2$ trap. This can be practically implemented by flowing additional helium through the $^{11}\text{CO}_2$ trap at room temperature or during the heating step, prior to $^{11}\text{CO}_2$ desorption.

Another interesting observation is that on average, only 53% of the C-11 was accounted for during runs performed immediately after reduction of the molybdenum. Using a hand held Geiger counter, most of the unaccounted for carbon-11 was found to be on the molybdenum reactor. For subsequent runs (i.e. not immediately after reduction), an average of 96% of the expected carbon-11 was recovered from the reactor. It appears that freshly reduced molybdenum either reacts with carbon oxides or that carbon oxides remain adsorbed on the surface.

Clearly the state of the molybdenum plays an important role in the reduction of carbon dioxide to carbon monoxide. To gain a better understanding of surface pretreatment and the effect of flow and temperature on CO_2 reduction by molybdenum, further experiments were carried out with cold $^{12}\text{CO}_2$ at UBC. In parallel to these experiments, a study of equilibrium using Aspen was carried out for various systems containing molybdenum, molybdenum oxides, molybdenum carbides, oxygen, hydrogen, carbon, carbon oxides and water.

4.3 Equilibrium computer simulations of systems containing molybdenum

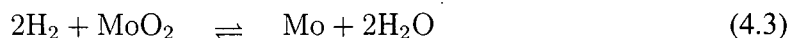
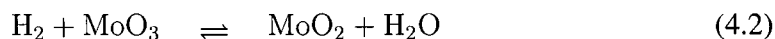
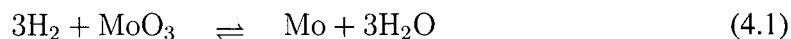
Equilibrium of molybdenum oxidation with oxygen and molybdenum trioxide reduction with hydrogen reduction were examined, as was the equilibrium of molybdenum oxidation with carbon dioxide using a process simulator. Two process simulators were available in the Department of Chemical & Biological Engineering; Aspen [76] and Hysys [77]. Aspen was

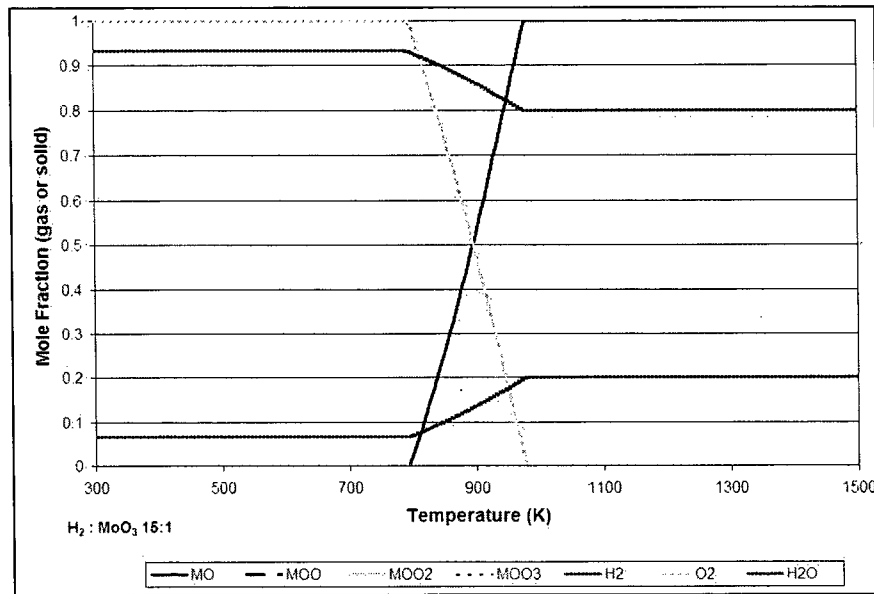
selected due to its broad component database which includes solids such as molybdenum. In order to obtain equilibrium data, a Gibbs reactor was setup using Aspen. All relevant components available from the database were included for each simulation. Using the sensitivity study feature of Aspen, equilibrium data was generated for a wide range of temperatures. Further details about setting up the Aspen simulations are described in the appendix, on page 100. A good overall agreement between Aspen produced simulation data with published equilibrium data for the system containing Mo, CH₄, C, H₂ and Mo₂C is demonstrated.

4.3.1 Reduction of MoO₃ with H₂

Aspen generated equilibrium data for the system containing H₂, O₂, H₂O, MoO₃, MoO₂, MoO and Mo is presented in figure 4.2, based on an initial H₂: MoO₃ ratio of 15:1, and at atmospheric pressure. MoO₃ is reduced to MoO₂ at room temperature. At 800 K, MoO₂ begins to form Mo, until it is completely reduced at ~1000 K. Based on simulation results, it appears that the reduction of MoO₃ to Mo proceeds through two reactions, via the intermediate molybdenum dioxide, as shown in eqs. 4.2 and 4.3.

In practice, a large excess of H₂ will be present, since a continuous stream of hydrogen would flow over a fixed amount of molybdenum. Figure 4.3 illustrates the effect of increasing the amount of H₂ from stoichiometric feed amounts (for complete reduction according to eq. 4.1) up to an excess with H₂: MoO₃ molar ratio of 240:1. The effect of increasing the excess of hydrogen is to shift the equilibrium to metallic molybdenum at a lower temperature.





Initial ratio of H₂: MoO₃ of 15:1, at atmospheric pressure

Figure 4.2: Equilibrium compositions of Mo-MoO-MoO₂-MoO₃-H₂-O₂-H₂O from 300 to 1500 K

4.3.2 Oxidation of Mo with O₂

Equilibrium of oxygen and molybdenum

Using the same component database and Gibbs reactor as for MoO₃ reduction, equilibrium data for Mo oxidation was obtained. The data generated from Aspen indicates that Mo would be completely oxidized to MoO₃, as illustrated in eq. 4.4, at temperatures above 273 K, for stoichiometric and larger amounts of O₂.



Equilibrium of carbon dioxide and molybdenum

Similar to above, simulations were carried out using Aspen to obtain equilibrium curves to better understand the effect of temperature on interaction between Mo and CO₂. To cover all possible reactions, the components added to the simulation were the following: He, Ar,

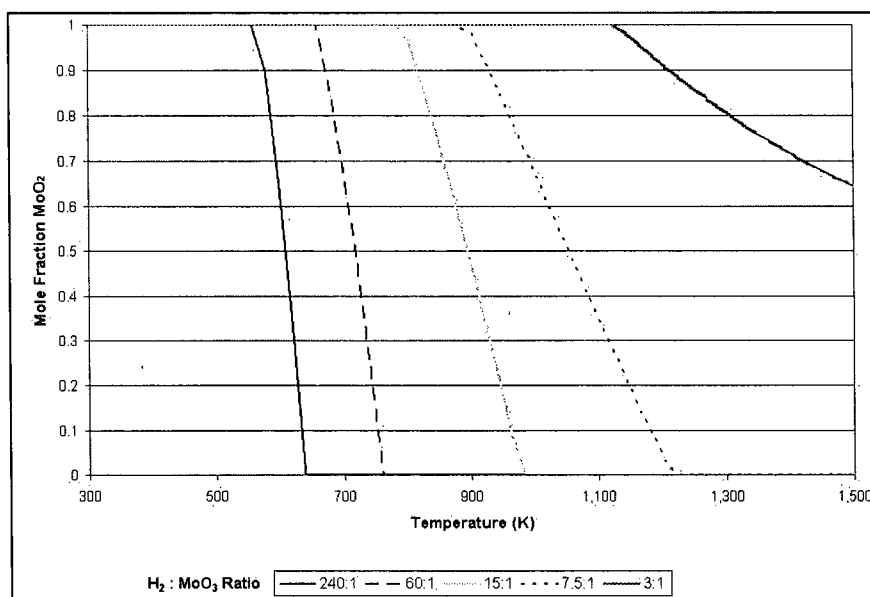


Figure 4.3: Equilibrium mole fraction of MoO_2 for different $\text{H}_2:\text{MoO}_3$ ratios from 300 to 1500K

CO , CO_2 , C , Mo , MoO , MoO_2 , MoO_3 , MoC and Mo_2C . The gas feed stream was set to contain 50 ppm CO_2 in argon, with an excess molybdenum, at atmospheric pressure. The resulting data is illustrated in figure 4.4. The compounds present at equilibrium are Mo , CO , CO_2 , Mo_2C , MoO_2 . Three distinct stages can be observed. Between 500 K and 800 K, equimolar amount of MoO_2 and Mo_2C are formed, most probably according to eq. 4.5, and no carbon is present in the form of carbon oxides. As the temperature increases above 800 K, the amount of Mo_2C relative to MoO_2 decreases, until no Mo_2C is present at 910 K. At this point the amount of CO is the highest, corresponding to 73% conversion of CO_2 . Above 910 K, it appears that the reaction proceeds according to eq. 4.6.



To verify these reactions independently, Aspen simulations were carried out for the

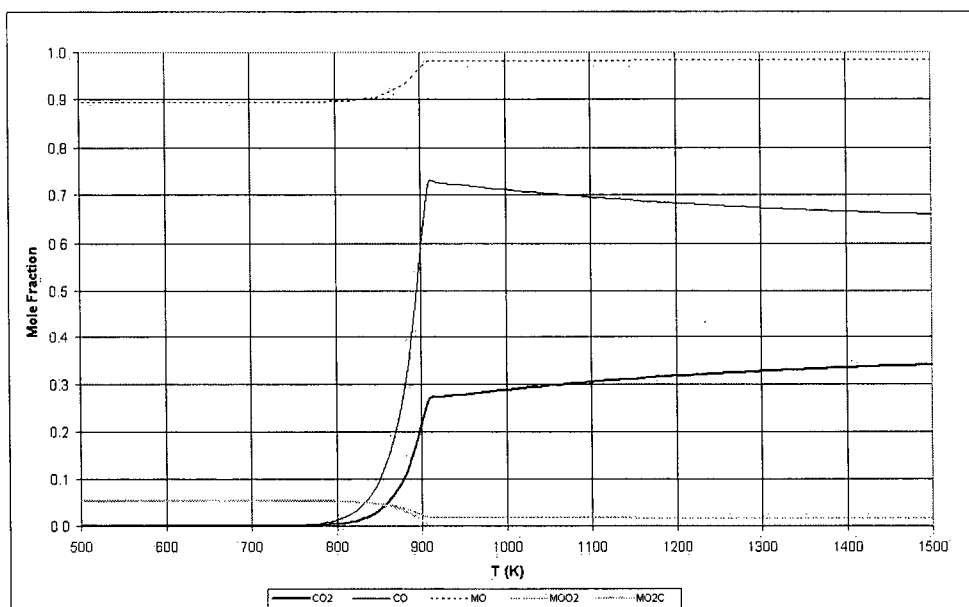


Figure 4.4: Equilibrium of composition of Mo-MoO₂-Mo₂C-CO₂-CO

same components as above, but using an equilibrium reactor, for which the chemical reaction can be specified. The feed gas stream was set to contain 50 ppm CO₂ in argon, with an excess molybdenum in the solid feed stream, both at atmospheric pressure. For an equilibrium reactor based on eq. 4.5 only, the resulting equilibrium curve is illustrated in figure 4.5. For temperatures below 800 K, no carbon dioxide is present, the only compounds present are dimolybdenum carbide and molybdenum dioxide, which confirms that the lower temperature plateau in figure 4.4 proceeds according to eq. 4.5. For an equilibrium reactor based on eq. 4.6, the resulting equilibrium curve is illustrated in figure 4.6. At 500 K, carbon monoxide is present with a molar fraction just below 0.90. As temperature increases, the molar fraction of carbon monoxide gradually decreases to 0.66 at 1500 K. The high temperature plateau in figure 4.4 follows the same exponential decrease, which confirm that the high temperature stage proceeds according to eq. 4.6.

Further simulations were carried out to explore the effect of varying the CO₂ concentration on the equilibrium amounts of CO present, as represented in figure 4.7. The equilibrium data is represented in terms of conversion of CO₂ to CO, which was calculated by

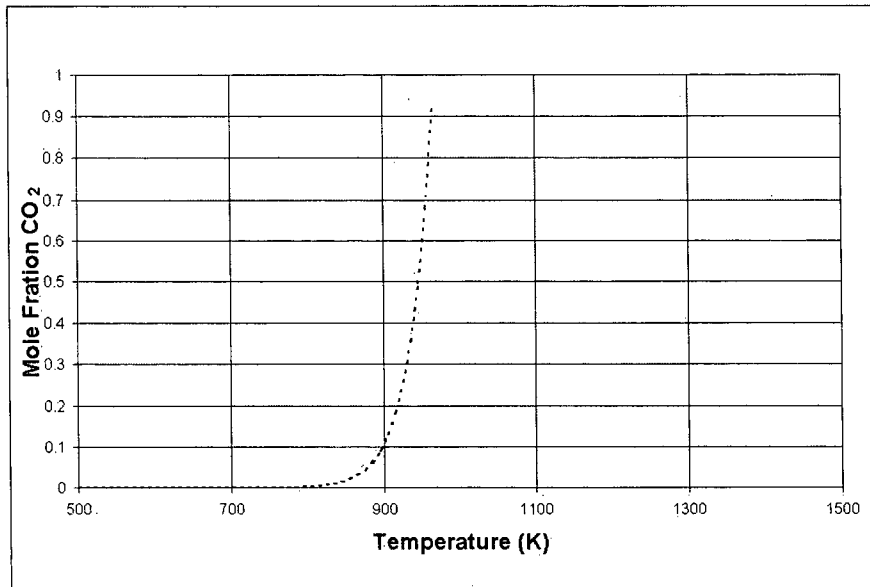


Figure 4.5: Equilibrium molar fraction of CO₂ from eqs. 4.5

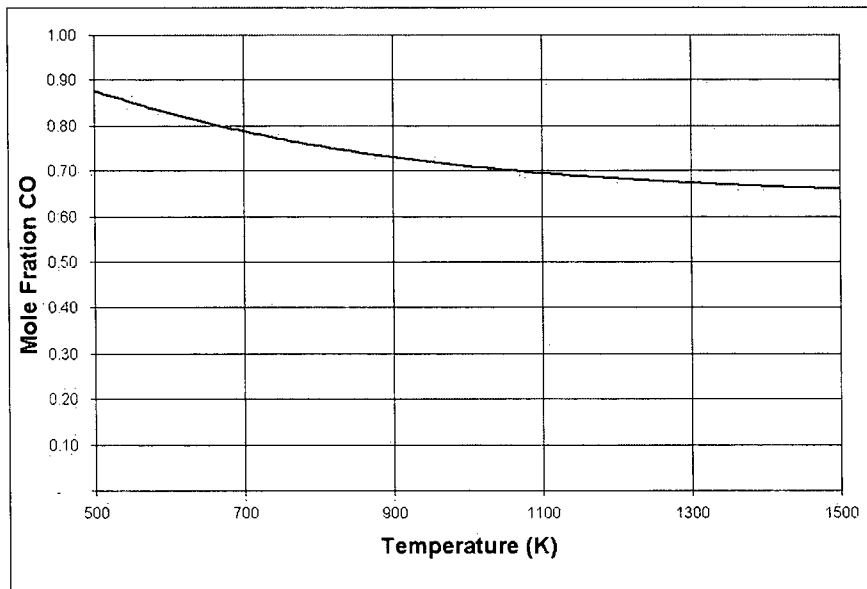


Figure 4.6: Equilibrium molar fraction of CO from eqs. 4.6

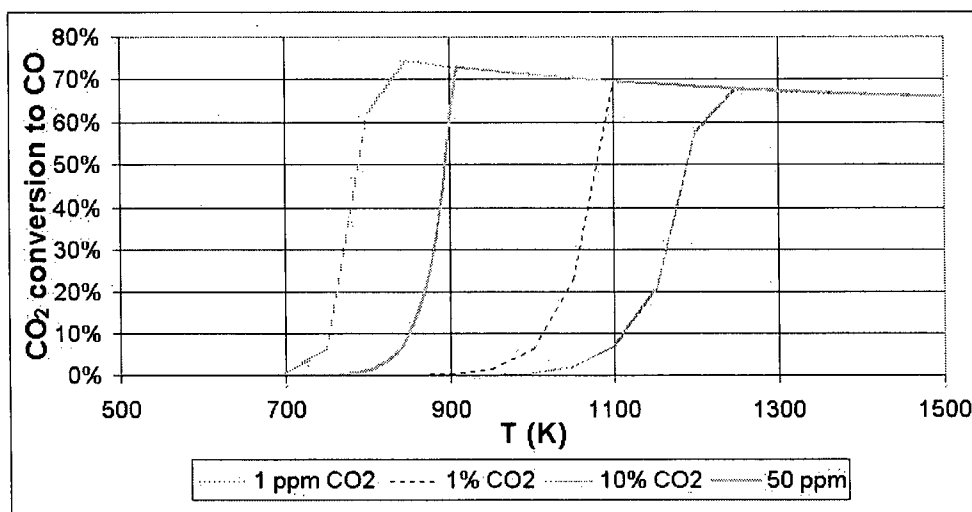


Figure 4.7: Conversion of CO₂ to CO vs. temperature for different CO₂ concentration, based on Aspen equilibrium data

dividing the equilibrium amount of CO by the initial amount of CO₂. The shape of the curve follows a similar pattern for each CO₂ concentration. The three stages described above are present in all cases. The temperature at which CO₂ conversion reaches a maximum increases with increasing carbon dioxide concentration. For 1 ppm carbon dioxide, the maximum CO₂ conversion to CO occurs at 850 K, while for 10% carbon dioxide the maximum conversion occurs at 1250 K.

Cold experiments were performed with 50 ppm carbon dioxide. Accordingly, the experimental temperature range was selected to cover the three stages described above, i.e. from 600 to 1150 K.

4.4 Cold experiments: reaction of CO₂ and Mo

4.4.1 Introduction

CHUS “hot” testing facilities provide a relatively simple method to quantify conversion of trace amounts of ¹¹CO₂. However, due to limited availability of the CHUS facilities and the financial burden associated with their use, “cold” testing with non-radioactive CO₂ was

done to better understand the factors affecting the reduction of CO₂ with molybdenum. Temperature programmed reduction of carbon dioxide with molybdenum and the effect of flow rate on the reduction of carbon dioxide with molybdenum were studied.

4.4.2 Materials and methods

During typical productions of carbon-11 compounds, the concentration of CO₂ ranges from 1-2000 ppm in the feed gas, as demonstrated in the appendices on page 105. A 50 ppm CO₂ feed gas was selected, consisting of certified 51.4 ppm CO₂ in helium, which was contained in a 100 bar standard laboratory size gas cylinder.

The gas flow rate was controlled by a mass flow controller (MKS instruments) for flow rates below 70 cm³/min (STP) and by an adjustable needle valve correlated flowmeter (Cole-Parmer) for higher flowrates. Calibration of both flow control devices was done using the soap-bubble method, and calibration curves are included in the appendices, on page 91.

Manual 2-way valves (Swagelok) were placed at the inlet and at the outlet of the reactor. The reactor consisted of a 400 W ceramic tubular heater (Omega Heating) in which a glass tube was placed, which contained 2.3 g molybdenum wire previously described, covering a length of 10 cm. A K-type thermocouple was placed in the middle of the ceramic heater, and a second K-type thermocouple was placed inside the reactor, on the molybdenum wire. Temperature was controlled with a manual operated thermostat (Omega).

The temperature profile along the reactor was obtained by measuring the temperature at 2 cm intervals from the entrance of the reactor. Temperature profile of the reactor showed a variation of over 160°C over the molybdenum covered length of the reactor for a setpoint of 740°C, as illustrated in the appendices, on page 98. The addition of quartz wool plugs on either end of the ceramic heater improved the temperature profile along the reactor, reducing the temperature variation of the molybdenum covered length to less than 60°C.

The product gas stream was connected to a 6-port sampling valve (VICI). The 6-port

valve was also connected to a waste stream, to a 2 cm³(STP) sample loop, to a hydrogen supply and to the the inlet of the gas chromatograph.

A Varian 3600 gas chromatograph was used, equipped with a a flame ionization detector (FID). The column used on the gas chromatograph was a 3 m long, 3.2 mm outer diameter column, packed with 60-80 mesh carbon molecular sieve. FID detectors are not very sensitive to carbon monoxide, and are not useful for detection of carbon dioxide. A well known method of analyzing trace amounts of carbon oxides using FID is to first convert the oxides to methane using a nickel catalyst. Near quantitative conversion of carbon monoxide and carbon dioxide to methane can be accomplished by flowing the sample gas containing the carbon oxides over a nickel catalyst with excess hydrogen, at 370-450°C. Accordingly, a methanizer was built. A 15 cm long aluminum heater block was built at Ebco to accommodate a 6.3 mm diameter 175 W cartridge heater (Omega), a 3.2 mm diameter tube and a 1.6 mm diameter K-type thermocouple (Omega). A 3.2 mm diameter stainless steel tube was packed with 0.34 g of a mixture of 15% commercially available nickel on alumina powder (< 60 µm) and 85% activated alumina, 100-120 mesh size. The excess nickel powder was shaken off prior to packing the tube, after which quartz wool plugs were placed at both ends of the tube. The nickel packed tube was placed in the aluminum heating block. Swagelok fittings were placed on either end of the tube. The methanizer was placed in the gas chromatograph, in between the separation column and the flame ionization detector. The temperature was controlled with a manual thermostat (Omega). Calibration curves for carbon monoxide and carbon dioxide are given in the appendices, on page 93.

4.4.3 Experimental set-up

The flow diagram for the experimental setup used for the reduction of CO₂ to CO is illustrated in figure 4.8.

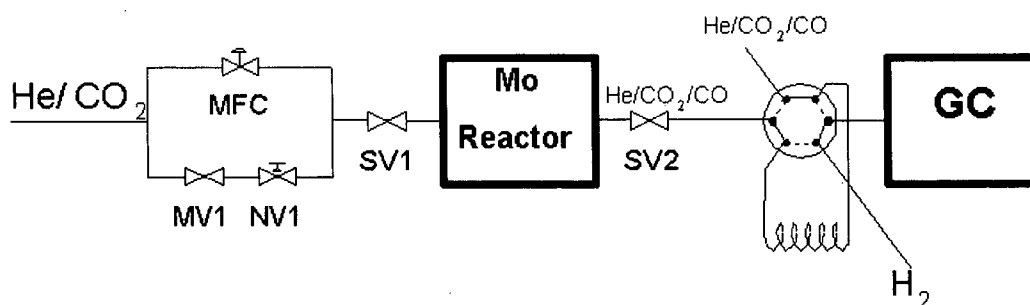


Figure 4.8: Experimental flow-diagram for the reduction of CO_2

4.4.4 Experimental procedure

Preliminary experiments, described in section 4.2, gave less than 10% conversion of [^{11}C]carbon dioxide to [^{11}C]carbon monoxide, most probably due to the presence of oxygen which oxidized the molybdenum to molybdenum trioxide.

Aspen equilibrium data suggests that the temperature at which molybdenum oxides are reduced to molybdenum metal depends on the molar ratio of hydrogen to molybdenum. For a ratio of H_2 :Mo of 240, complete reduction to molybdenum occurs at 400°C . For a ratio of H_2 :Mo of 7.5, complete reduction to molybdenum occurs at 900°C . In the reactor used, 2.3 g of molybdenum wire was placed in a length of 10 cm within the 6.3 mm inner diameter quartz reactor. Assuming only the exposed surface atoms are available for reaction, this corresponds to a molar ratio for H_2 :Mo of 130. At this molar ratio, Aspen generated data indicates that 425°C would be sufficient for reduction to molybdenum.

There is a general agreement that the reduction of molybdenum trioxide with hydrogen to molybdenum metal is a two step process, forming molybdenum dioxide as intermediate, though the exact temperature at which reduction is reported varies. The reduction of molybdenum trioxide to molybdenum dioxide is reported to occur between 350 - 600°C while the reduction of molybdenum dioxide to molybdenum is reported to occur between 500 - 1150°C . Lee et al. [54] prepared molybdenum by TPR of 0.5 g MoO_3 powder with pure hydrogen at $50 \text{ cm}^3/\text{min}$, from 300°C to 700°C , increasing temperature $60^\circ\text{C}/\text{h}$.

Carbon monoxide is more strongly adsorbed on freshly reduced molybdenum carbide than unreduced molybdenum carbide [54]. Iwasawa et al. [55] observed deposition of small amounts of carbon on molybdenum fixed on alumina, after it had been reduced with hydrogen at 500°C for 5 h. Although no data was provided for adsorption of carbon monoxide and carbon dioxide on freshly reduced molybdenum, there is a chance that adsorption is higher on freshly reduced molybdenum as well. Lee et al. [54] suggested to passivate dimolybdenum carbide with 1% oxygen at room temperature prior to removal of carbide from the reactor for surface analysis.

Following Lee's [54] procedure, temperature programmed reduction was performed on the molybdenum wire, from 300 to 700°C with a temperature increase of 60°C/h, with an additional 12 hours of isothermal reduction at 700°C. UHP hydrogen, which contained 50 ppm of CO and 50 ppm CO₂ was used as reduction media. Following cooling, the molybdenum wire was passivated with UHP compressed air, at room temperature, for one hour.

Experiments were carried out using the experimental set-up illustrated in figure 4.8. The experiments were separated in two parts, temperature programmed reaction and flowrate programmed reaction.

For the temperature programmed reaction experiments, the gas stream was fed through the reactor at a fixed pressure of 2 bar and a fixed flowrate of 4 cm³/min (STP). The temperature of the molybdenum wire was varied from 331 and 883°C, in increments of approximately 60°C. At each temperature, 2 cm³ samples of the gas product were analyzed using GC for quantification of carbon dioxide and carbon monoxide.

For the flowrate programmed experiments, the molybdenum wire was kept at a fixed temperature of 825°C and the feed gas was kept at constant pressure of 2 bar. The flowrate of the feed stream containing 50 ppm CO₂ in helium was varied from 5 to 1642 cm³/min (STP). At each flowrate, a 2 cm³ sample of the gas product was analyzed using GC for quantification of carbon dioxide and carbon monoxide.

4.4.5 Results and discussion

During the reduction of molybdenum, water vapor was visible at the outlet of the reactor, indicating that molybdenum oxides were present initially. At the end of the isothermal reduction at 700°C, water vapor was no longer visible. There was some concern that molybdenum carbide may have been formed, due to the presence of 50 ppm carbon monoxide and carbon dioxide in the hydrogen gas. GC analysis of the product stream showed a single peak, methane, indicating that carbon oxides reacted with hydrogen to form methane. Additional Aspen equilibrium simulations indicated that the only components in the product stream at equilibrium at 700°C are molybdenum, methane, water and hydrogen. The molybdenum wire had a shiny metallic finish, characteristic of molybdenum metal. It was concluded that molybdenum oxides were present and that they were reduced to molybdenum.

The effect of temperature on the ratio of CO to total carbon oxides in the product stream from a feed stream containing 50 ppm CO₂ reacting with molybdenum from 331 and 883°C is illustrated in figure 4.9. Three distinct stages can be observed:

1. from 331 to 600°C, a plateau with average CO/(CO₂+CO) of 20%,
2. from 600 to 700°C, an abrupt increase from 20% to over 70% CO/(CO₂+CO)
3. from 700 to 883°C, a plateau with average CO/(CO₂+CO) of 71%.

A similar abrupt increase in carbon monoxide generation was observed by Zeisler et al. [40] at 825°C (see figure 2.3), for reaction of ¹¹CO₂ with molybdenum, and by Solymosi et al. [66] at 600°C (see figure 2.4), for reaction of carbon dioxide with molybdenum carbide.

Aspen generated equilibrium data shows an abrupt increase in the conversion of CO₂ to CO, as illustrated in figure 4.7. The most notable difference between Aspen generated equilibrium data and experimental data is the fact that Aspen data suggests the absence of carbon oxides in the lower temperature plateau. However, experimental data from this study

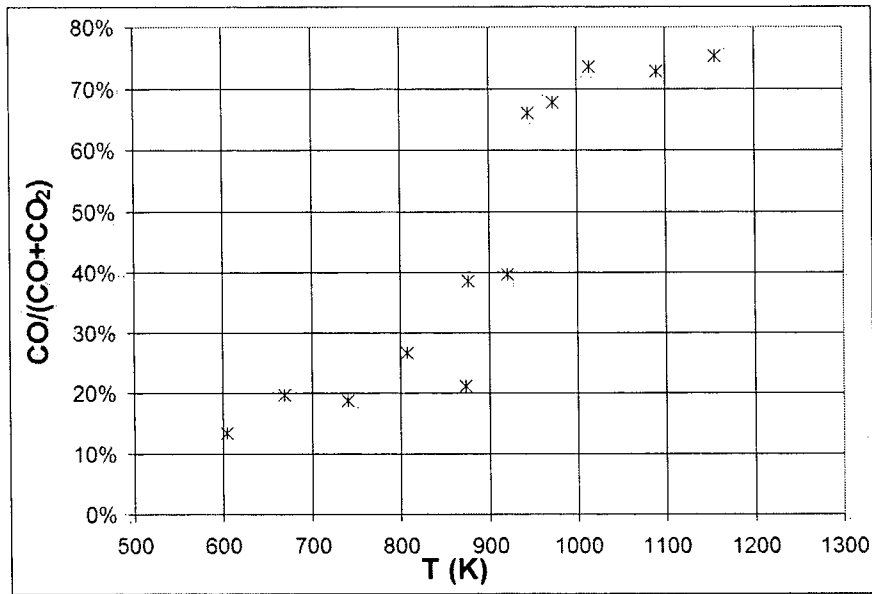


Figure 4.9: Effect of temperature on reaction of CO₂ and Mo, at 4 cm³/min and 2 bar

and others indicate that carbon monoxide is present at the lower temperature plateau. Aspen equilibrium data suggests that in the lower temperature plateau all the carbon dioxide reacts with molybdenum to form dimolybdenum carbide and molybdenum dioxide, as illustrated in figure 4.5. However, experimental results show that both carbon dioxide and carbon monoxide are present between 331 to 600°C. Overall, Aspen appears to be a good tool to determine the general profile for equilibrium conversions of carbon dioxide to carbon monoxide as a function of temperature for the conditions of this study, in particular for the second and third temperature stages described above.

The effect of flowrate on the ratio of CO to total carbon oxides in the product stream from a feed stream containing 50 ppm CO₂ reacting with molybdenum at 825°C is illustrated in figure 4.10. Between 5 and 70 cm³/min (STP), there is no significant change in the ratio of carbon monoxide to total carbon oxides, averaging 76%. At 70 cm³/min (STP), the ratio of carbon monoxide to total carbon oxides decreases exponentially from 74% to less than 2% at approximately 1250 cm³/min (STP).

The total amount of carbon oxides in the product stream exceeded the 51.4 ppm carbon

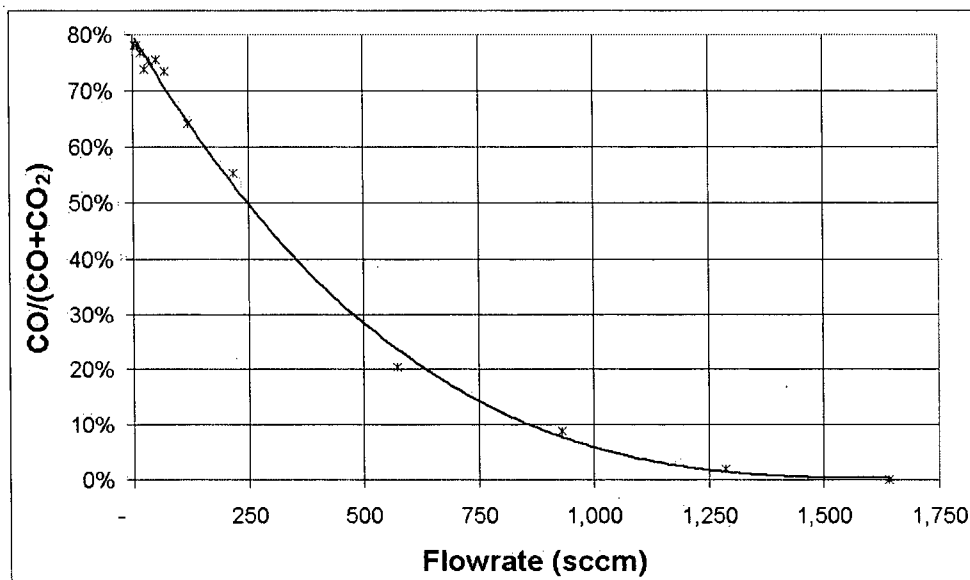


Figure 4.10: Effect of flowrate on reaction of CO₂ and Mo at 825°C and 2 bar

dioxide contained in the feed stream. For this reason, both figure 4.9 and 4.10 were plotted as a ratio of carbon monoxide to total carbon oxides. Figures 4.11 and 4.12 show the total amount of carbon oxides in the product stream, as a function of temperature and flowrate respectively.

In figure 4.11, the data follows a similar trend as the curve in figure 4.9. There is an initial increase in total carbon oxides in the product stream from 50 ppm to around 120 ppm, from 340 to 400°C. Between 400 and 600°C, the amount of carbon oxides gradually decreases from 120 ppm to 90 ppm. Between 600 and 800°C, there is a much larger increase from 90 to 450 ppm carbon oxides. From 800 to 880°C, the amount remained constant at 450 ppm.

In figure 4.12, the total amount of carbon oxides decreases exponentially from 75 ppm down to around 50 ppm. Considering that the flow experiment were done after the temperature experiments, this decrease from 75 to 50 ppm appears to be the tail end of the larger peak seen in figure 4.11, beginning at 600°C.

There are two possible explanations for the source of this additional carbon. The first possibility is that molybdenum carbide may have formed at the lower temperature during

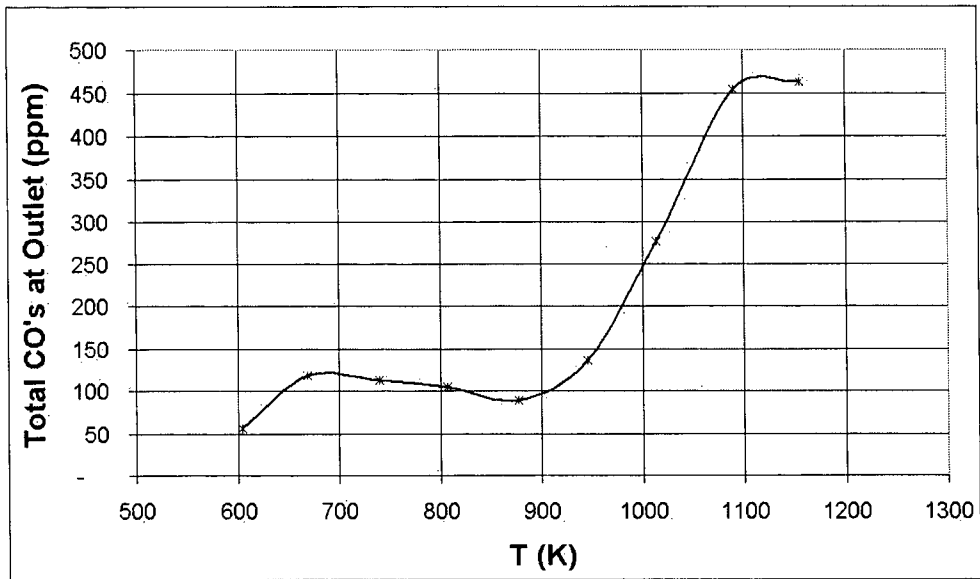


Figure 4.11: Total carbon oxides as a function of temperature.

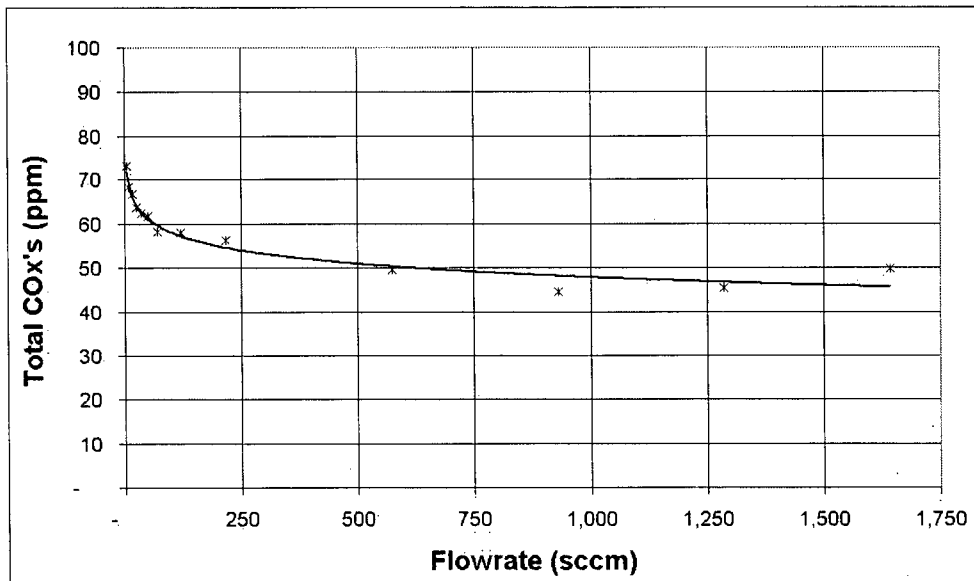


Figure 4.12: Total carbon oxides as a function of flowrate.

start-up of the apparatus and reacted with carbon dioxide and/or molybdenum dioxide to form carbon monoxide. The second possibility is that carbon dioxide and/or carbon monoxide remained adsorbed on the molybdenum surface prior to experiments and were released during experiments.

Aspen generated equilibrium data suggests that Mo_2C and MoO_2 are formed by reacting molybdenum with carbon dioxide, from room temperature to 500°C . However, published data on formation of molybdenum carbide from carbon monoxide with molybdenum dioxide, according to the reversible eq. 2.14 on page 26, proceeds at temperatures above 565°C [57]. The formation of molybdenum carbide by reaction of CH_4 in hydrogen with molybdenum trioxide was reported to occur above 500°C . Thus, regardless of how molybdenum carbide is formed, it appears that the temperature must be over 500°C and that the carbon source must react with a molybdenum oxide. In Figure 4.11, there is always more than 51.4 ppm total carbon in the product stream, indicating that carbon dioxide probably did not react with molybdenum to form molybdenum carbide. Thus, the possibility that molybdenum carbide was the source of additional carbon seems highly improbable.

Considering the second possibility, numerous studies have found CO and carbon adsorption on molybdenum compounds is significant, in particular after reduction with hydrogen [54, 55]. During preparation of the molybdenum, after TPR reduction, some carbon dioxide and carbon monoxide may have remained adsorbed on the freshly reduced molybdenum while cooling to room temperature. During start-up of the experiments, helium containing 51.4 ppm carbon dioxide was flowing through the reactor. Since up to 120 ppm carbon dioxide was measured in the product stream, it is highly probable that some carbon dioxide was previously adsorbed on the molybdenum surface. The adsorption of carbon monoxide and carbon dioxide on the molybdenum surface during start-up and pretreatment seems to be the most likely source of additional carbon measured during experiments.

The components molybdenum, molybdenum oxides, molybdenum carbides and carbon oxides constitute a complex system. The equilibrium data generated by Aspen provided

a good prediction of the achievable yield of carbon monoxide. For the high temperature plateau, the reduction of CO_2 to CO proceeds according to eq. 4.6, oxidizing molybdenum to molybdenum dioxide.

Chapter 5

Experimental: Methanol synthesis

5.1 Introduction

In order to estimate the requirements for the production of [^{11}C]methanol via a gas phase catalytic process, a series of experiments have been conducted with non-radioactive carbon monoxide. Although commercial methanol production involves a catalytic gas phase process, no practical procedure is currently available for the production of [^{11}C]methanol. The industrial production of methanol uses catalysts such as $\text{Cu/ZnO/Al}_2\text{O}_3$ that are prepared by co-precipitation and activated with 1-3% hydrogen at 250-290°C prior to use. The feed gas is normally syngas, which contains CO , CO_2 , CH_4 and H_2 , with the carbon dioxide acting as an oxidizing agent.

This study aimed at determining the suitability of the catalytic gas phase procedure for the production of [^{11}C]methanol. Activation and precondition of a copper zinc oxide catalyst were evaluated. The effect of pressure, temperature and flowrate of the feed gas on the methanol yield were studied and a kinetic model was generated. The model was used to establish optimal condition and estimate the potential yields of [^{11}C]methanol production via a catalytic gas phase method.

5.2 Materials and methods

In order to be consistent with conditions encountered during carbon-11 labelling procedures, a 50 ppm CO feed gas was selected (see page 105). It consisted of certified 50 ppm CO in hydrogen, which was supplied in a 100 bar standard laboratory size gas cylinder. UHP helium gas, contained in a 100 bar standard laboratory cylinder, was used as inert sweep gas.

The gas flow rate was controlled by a mass flow controller (MKS instruments) for flow rates below $70 \text{ cm}^3/\text{min}$ and by an adjustable needle valve correlated flowmeter (Cole-Parmer) for higher flowrates. Calibration of both flow control devices was done using the soap-bubble method, for which calibration curves are included in the appendices, on page 91.

A manual 3-port valve (Swagelok) was placed at the inlet of the reactor, to select either helium or the feed gas. The reactor consisted of a 400 W ceramic tubular heater (Omega Heating) in which a 6.3 mm inner diameter stainless steel tube was placed, which contained the copper based catalyst, covering a length of 6 cm. A K-type thermocouple was placed in the middle of the ceramic heater, and a second K-type thermocouple was placed inside the reactor, in contact with the catalyst. The reactor temperature was controlled with a manual operated thermostat (Omega). Quartz tubes, 6.3 mm outer diameter with 1 mm inner diameter, were placed on both ends of the reactor to reduce the void space and the time required for the product gas to flow through the remaining portion of the reactor. Glass wool plugs were placed on both ends of the heater, to improve temperature uniformity. The resulting temperature profile of the reactor is included in the appendices. The outlet of the reactor was connected to a pressure regulator to maintain downstream pressure below the rating of the flow control devices. The product stream was also connected to a 6-port sampling valve (VICI). The 6-port valve was connected to a waste stream, a 2 cm^3 sample loop, a hydrogen supply and the inlet of a varian 3600 gas chromatograph, equipped with a flame ionization flame detector (FID). The GC was equipped with a 3 m long stainless

steel column (1.6 mm inner diameter) packed with 60-80 mesh poropak. Using a stream of helium saturated with methanol, a calibration curve was generated and is illustrated in the appendices, on page 93.

5.2.1 Cu/ZnO catalyst preparation

Copper nitrate pentahemihydrate, $\text{Cu}(\text{NO}_3)_2 \cdot 2.5\text{H}_2\text{O}$, and sodium carbonate were obtained from Aldrich. Zinc nitrate hexahydrate, $\text{Zn}(\text{NO}_3)_2 \cdot 6\text{H}_2\text{O}$ was obtained from JT Baker.

The procedure used for the preparation of the copper zinc oxide catalyst was based on the method described by Herman et al. [71]. A 1.0 M solution of copper nitrate was prepared by dissolving 21.6 g copper nitrate pentahemihydrate in 92.9 mL distilled water. Similarly, a 1.0 M zinc nitrate solution was prepared by dissolving 64.5 g in 216.7 mL distilled water. These nitrate solutions were mixed to obtain a 30:70 molar ratio of Cu:Zn. A 1.0 M solution of sodium carbonate was prepared by dissolving 50 g Na_2CO_3 in 472 mL distilled water and was added dropwise to the 310 mL metal nitrates solution at 90°C , until the pH was raised from 2 to 7.0. The titration took 5 h and consumed approximately 360 mL sodium carbonate. Following a 12 h digestion at room temperature, the turquoise precipitate was filtered over glass frit and dried overnight at $85\text{-}105^\circ\text{C}$. The subsequent calcination of the copper/zinc carbonates was carried out in air by heating from 150 to 350°C in 2 h, with the maximum temperature maintained for 4 h. The resulting copper/zinc oxides were pelletized from an aqueous slurry, dried at ambient temperature and crushed and screened to a uniform size of $650 \pm 200 \mu\text{m}$. Samples of 2 g were placed in the reactor, covering a length of 6 cm. The catalyst was reduced under flow of 2% hydrogen in helium, for 12-16 h at 250°C and 1 bar. A standard BET method was used for the determination of surface area from argon adsorption at -196°C and the surface area of the reduced, used catalyst, was $30.3 \text{ m}^2/\text{g}$. This is in the same range as measurements made by Herman et al., who reported a surface area of $37.1 \text{ m}^2/\text{g}$ for catalyst prepared by a similar method, and used under commercial methanol synthesis conditions [71].

5.3 Experimental procedure

The flow diagram for the experimental setup used for the methanol synthesis reactor is illustrated in figure 5.1.

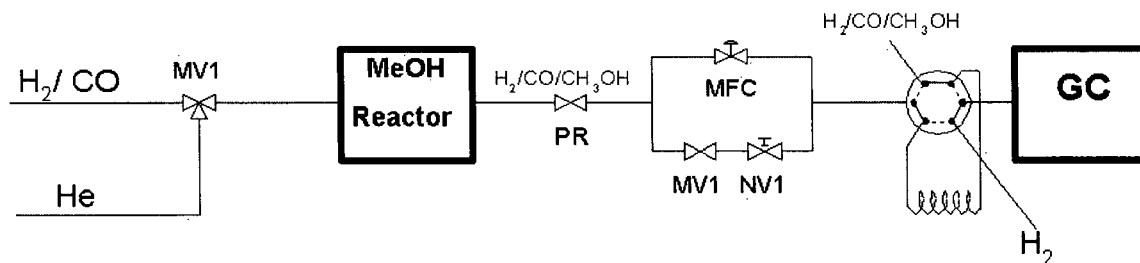


Figure 5.1: Experimental flow diagram for methanol synthesis

Commercial low pressure methanol synthesis is typically performed between 200-270°C and at 50 - 100 bar [78]. The practical pressure for [¹¹C]methanol production is about 50 bar, due to pressure rating of commonly used valves, tubing and fittings in automated synthesis units. Aspen generated equilibrium data for the system containing 50 ppm CO, is illustrated in figure 5.2, as conversion of CO to methanol as a function of temperature and pressure. The conversion was calculated by dividing equilibrium amounts of methanol by initial amounts of carbon monoxide. Due to the exothermic nature of methanol synthesis, as temperature increases, the equilibrium conversion of carbon monoxide to methanol decreases. For a given temperature, as the pressure increases, the equilibrium conversion of carbon monoxide to methanol increases. At 50 bar, equilibrium conversion of CO to methanol is 100% for temperatures below 180°C and decreases to 90% at 240°C.

5.3.1 Preliminary experiments: Cu/ZnO catalyst for CH₃OH synthesis

Preliminary experiments were performed using a continuous feed containing 50 ppm CO in hydrogen at temperatures ranging from 180 to 240°C, flowrates ranging from 2 to 126

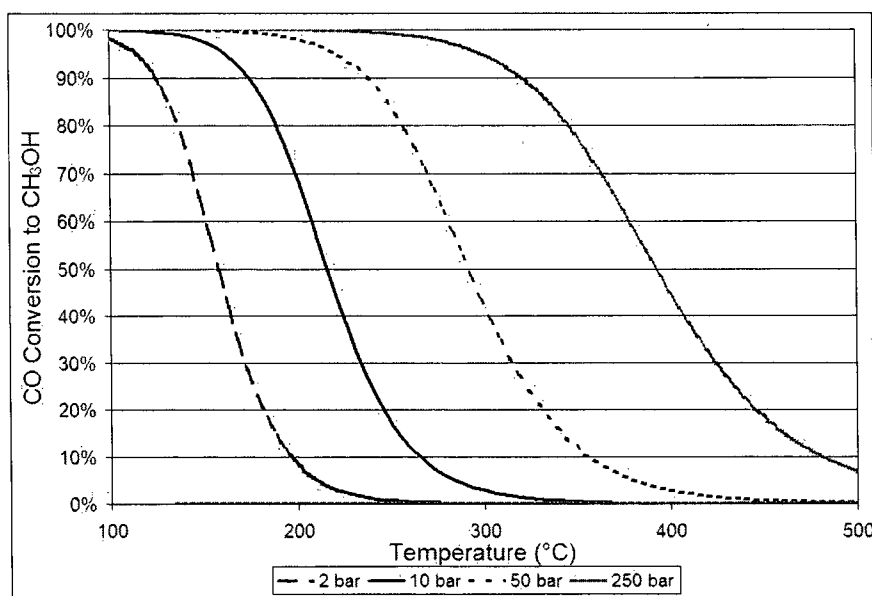


Figure 5.2: Aspen generated equilibrium conversion of 50 ppm CO to methanol, in hydrogen

cm³/min(STP) and pressures ranging from atmospheric to 2, 10 and 55 bar. The catalyst was pretreated by reduction at 250°C with 2% H₂ in helium for initial experiments. Subsequent experiments were performed using the same catalyst reduction conditions, however the catalyst was passivated by exposure to compressed air at 20°C. The feed gas, containing 50 ppm CO in hydrogen, was continuously fed through the reactor and the product stream gas was sampled every 5-30 minutes and analyzed using the gas chromatograph for quantification of methanol produced.

5.3.2 Effect of flowrate and temperature on CH₃OH synthesis

In the final application, with carbon-11, the process will be performed semi-batchwise. Accordingly, further experiments were carried out semi-batchwise. Prior to experiments, the catalyst was reduced as described previously. Prior to each experiment, the catalyst was oxidized by exposing it to compressed air at ambient temperature.

Effect of flowrate on methanol production:

The system was pressurized with helium at 55 bar, and flowmeter set to either 26, 93, 241, 468 and 935 cm³/min (STP). The reactor heater was turned on and set to 180°C, and samples of the product stream were analyzed using the gas chromatograph to ensure that no methanol was present. The feed gas was then switched to 50 ppm CO in hydrogen at 55 bar, for a period of 10-300 minutes giving between 0.3-0.9 cm³ (STP) carbon monoxide. Using the 6-port sampling valve, samples were analyzed using the gas chromatograph to quantify methanol concentration, typically at 2-5 minute intervals. After the predetermined CO feed time had elapsed, the tubing prior to reactor was vented and loaded with helium. When the reactor pressure reached 2 bar, the supply gas was switched to 2 bar helium and the flow rate was set to 126 cm³/min (STP). The product stream was sampled and analyzed using the gas chromatograph until methanol was no longer observed.

Effect of temperature on methanol production:

The system was pressurized with helium at 55 bar, and flowmeter set to 126 cm³/min (STP). The reactor heater was turned on and set to either 154, 178, 209, 224 or 240°C, and samples of the product stream were analyzed using the gas chromatograph to ensure that no methanol was present. Although commercial methanol synthesis is performed between 200-300°C, the experiments were limited to 240°C to avoid irreversible deactivation of the catalyst, which is reported to occur when catalyst is operated above 245°C and in the absence of an oxidizing agent [72, 71, 69]. The feed gas was then switched to 50 ppm CO in hydrogen at 55 bar, for a period of 20 minutes. The time was the same for all temperatures, and corresponds to 0.126 cm³ (STP) of carbon monoxide. Using the 6-port sampling valve, samples were analyzed using the gas chromatograph to quantify methanol concentration, typically at 2 minute intervals. After the predetermined CO feed time had elapsed, the tubing prior to reactor was vented and loaded with helium. When the reactor pressure reached 2 bar, the supply gas was switched to 2 bar helium and the flow rate was

set to 126 cm³/min (STP). The product stream was sampled and analyzed using the gas chromatograph until methanol was no longer observed.

5.4 Results and discussion:

5.4.1 Preliminary experiments: Cu/ZnO catalyst

Preliminary experiments were performed using a continuous feed of 50 ppm CO in H₂, at temperatures ranging from 180 to 240°C, flowrates ranging from 2 to 126 cm³/min(STP) and pressures of 2, 10 and 55 bar, using the reduced copper zinc oxide catalyst. No methanol was measured in the product stream under these conditions. The catalyst was then passivated with compressed air at 20°C, and the experiments were repeated. Experiments performed at 55 bar resulted in measurable amounts of methanol in the product stream. However, experiments performed at 2 and 10 bar using the same experimental conditions failed to produce any detectable amount of methanol in the product stream.

Using the passivated catalyst and operating pressure of 55 bar, further experiments were performed to measure the methanol produced as a function of time, for a continuous feed of H₂/CO. The amount of methanol in the product stream increases with time, then reaches a maximum, followed by a gradual decrease, as illustrated in figure 5.3. The methanol production appears to gradually stabilize, however there is no clear indication that a steady state is reached. For the experiment at 180°C, 55 bar and 2 cm³/min (STP), the concentration of methanol increases to a maximum of 45 ppm after about 150 minutes and then decrease to just under 18 ppm at 400 minutes. For the experiment at at 200°C, 55 bar and 26 cm³/min (STP), the concentration of methanol increases to a maximum of 12 ppm after about 75 minutes and then decreases to 7 ppm at 200 minutes.

The initial peak in methanol production is likely due to the presence of adsorbed carbon

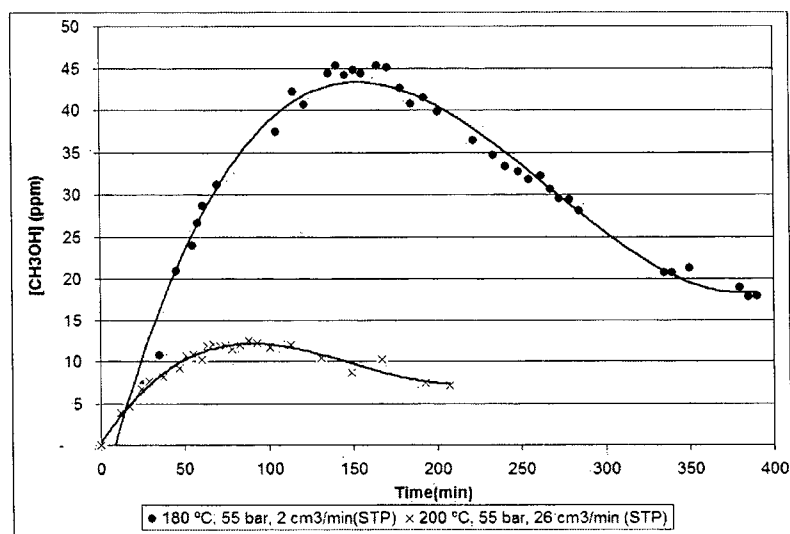


Figure 5.3: Methanol produced for continuous feed of H₂/CO

monoxide on the catalyst. While the reactor was heated to the operating temperature, the feed gas was 50 ppm CO in H₂. Thus carbon monoxide may have accumulated on the cold catalyst surface and reacted once the temperature was sufficiently high. Adsorption of carbon monoxide on a copper zinc oxide catalyst at ambient temperatures has been previously described [72, 74]. Klier [72] reports that for a catalyst with 30/70 ratio of Cu/ZnO, 1.7 mol of CO / g catalyst reversibly chemisorbs to the catalyst surface.

In summary, the preliminary results confirm that methanol can be produced from a feed stream containing 50 ppm CO in H₂ using an activated and passivated Cu/ZnO catalyst. These experiments also indicate that an operating pressure of 55 bar is adequate for methanol synthesis, while operating pressures below 10 bar are insufficient. The data suggests that carbon monoxide accumulated on the catalyst at ambient temperature and only appeared in the product stream as methanol once the operating temperature was reached. The experimental procedure for subsequent experiments was adapted accordingly: the catalyst was passivated prior to each experiment and the reactor was allowed to reach its operating temperature under helium flow before switching to the H₂/CO feed gas.

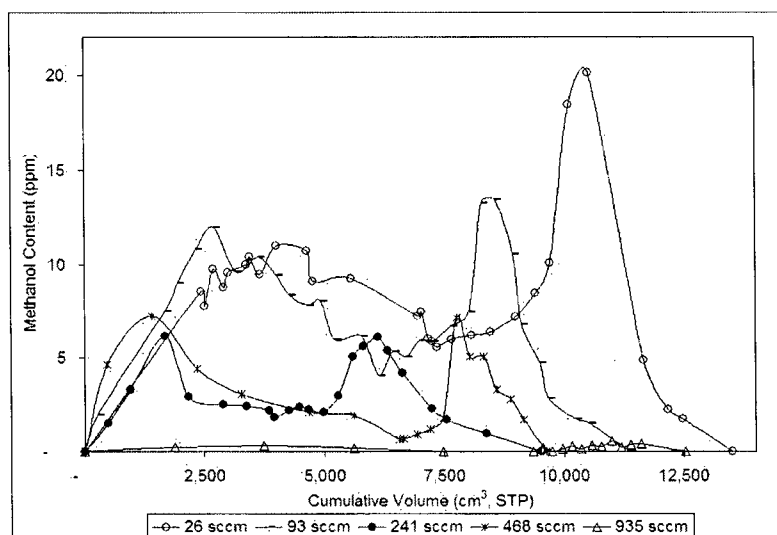


Figure 5.4: Semi-batch methanol produced, 180°C, 50 bar for different flowrates

5.4.2 Effect of flowrate and temperature on CH₃OH synthesis

For experiments performed under semi-continuous feed of H₂/CO, the concentration of methanol in the product stream vs. cumulative product stream volume is illustrated in figures 5.4 and 5.5.

Effect of flowrate on methanol production: Experiments were performed at 180°C, 55 bar and flowrates were varied between 26 and 925 cm³/min (STP). As the flowrate increases from 26 to 935 cm³/m (STP), the conversion of carbon monoxide to methanol decreases from 26% to 0.5% (Table on the next page). As can be seen in figure 5.4, the methanol is released in two distinct peaks. The first methanol peak was released while H₂/CO was fed to the reactor while the second peak was released during the helium purge, at 180°C, 126 cm³/m (STP) and 2 bar. As the flowrate increases from 26 to 935 cm³/m (STP), the percentage of methanol released during the helium purge phase decreases from 48% to 26% (Table on the following page).

The fact that the methanol produced is released in two distinct peaks, suggests that methanol synthesis has at least 2 rate limiting steps. One of the rate limiting steps is likely

Table 5.1: Effect of flowrate on conversion of CO to methanol (50bar, 180°C)

Flowrate (STP)	Methanol Yield	% methanol released during purge
26 cm ³ /min	26%	48%
93 cm ³ /min	21%	35%
240 cm ³ /min	10%	38%
468 cm ³ /min	8%	29%
935 cm ³ /min	0.5%	26%

Table 5.2: Effect of temperature on conversion of CO to methanol at 55bar, 126 cm³/min(STP)

Temperature	Methanol Yield
154°C	8%
178°C	14%
209°C	23%
224°C	25%
240°C	48%

associated with the rate of formation of methanol. The second methanol peak occurs when the flow is switched to helium and the pressure is dropped from 55 bar to 2 bar, indicating that methanol is more readily released at atmospheric pressure than at 55 bar. Moreover, the fact that the percentage of methanol released during the purging was higher at low flowrate, suggests that methanol desorption is a second rate limiting step, which is in agreement with earlier studies of the kinetics of low-temperature methanol synthesis [79].

Effect of temperature on methanol production: Experiments were performed at 126 cm³/min (STP), 55 bar and the temperature of the reactor was varied between 154 and 240°C. As the temperature increases from 154 to 240°C, the conversion of carbon monoxide to methanol increases from 8% to 48% (5.2). As can be seen in figure 5.5, most of the methanol produced is released in one major peak which occurred during the helium purge. Although at 240°C the methanol yield is the highest, a much larger volume of helium purge gas was required to release the methanol produced.

At first glance, it appears that methanol is released from the catalyst as a single peak for operating temperatures between 154-220°C. This suggests that methanol synthesis has one

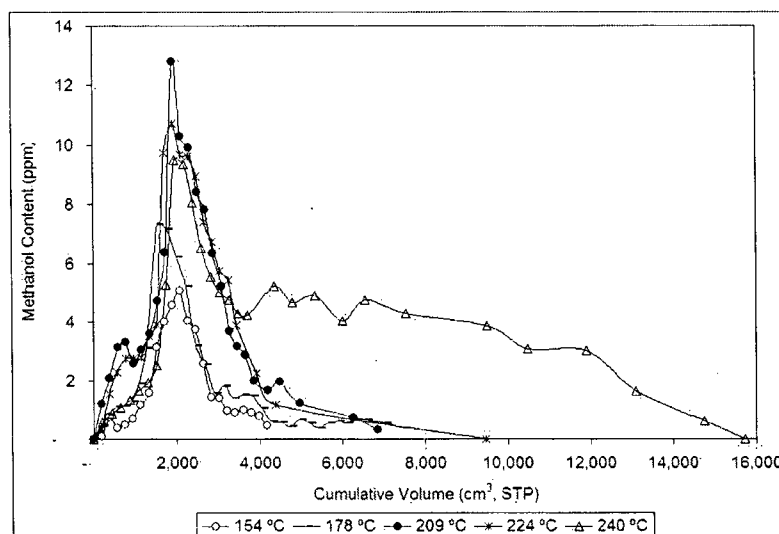


Figure 5.5: Semi-batch methanol produced, 120 cm³/min, 50 bar for different temperatures

rate limiting step. However, upon closer examination, three of the profiles reveal a small satellite peak appearing just before the major methanol peak. The amount of H₂/CO gas fed to the reactor in the temperature experiments was 2500 cm³ (STP), while up to twice as much was used in the flow experiments. In the latter experiments (figure (5.4)), the first methanol peak is released at about 2500 cm³ (STP), and the second peak is released during the helium purge at over 5000 cm³ (STP). During the temperature experiments, the major peak was observed while the reactor was purged with helium, at a cumulative volume of approximately 2000 cm³ (STP). Accordingly, the two peaks observed in the flow experiments would overlap in the temperature experiments. Thus, even though there are likely two or more rate limiting steps, only one peak appears in the temperature experiments. At 240°C, the methanol is released in a similar initial peak, but significant trailing suggests that an additional rate limiting step occurs. This is consistent with studies reporting that intra-particle diffusion limits the rate of methanol synthesis at temperature above 245°C [79, 80].

Table 5.3: Kinetic parameters for Leonov's model
For 154-240 °C, 55 bar and 26-935 cm³/min(STP)

	Value	units
k ₀	1.3E-4	mol/(cm ³ sbar ^{0.84})
E _a	73	kJ/mol

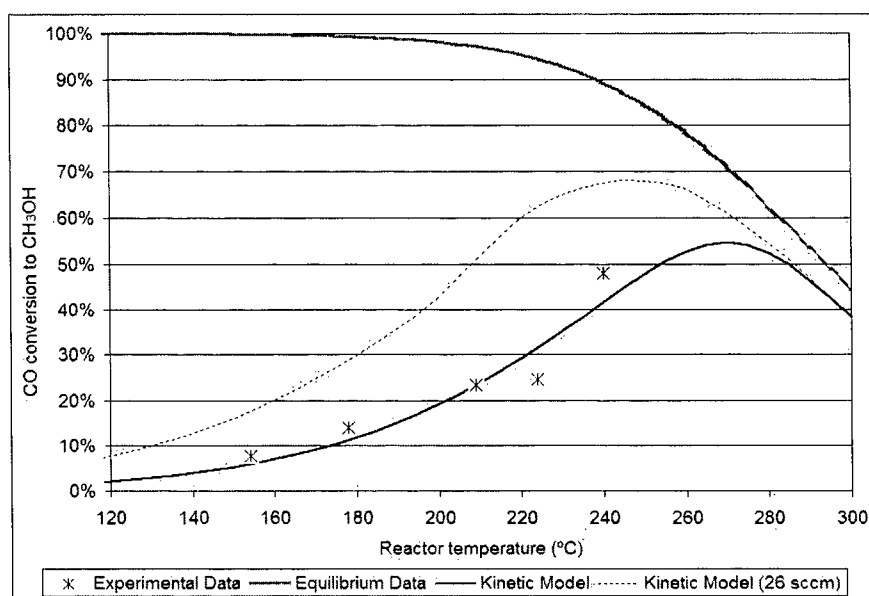
5.4.3 Kinetic Model

Leonov's proposed kinetic expression for methanol synthesis, illustrated in eq. 5.1, was used as a base kinetic expression to model the semi continuous CO/H₂ feed experimental results for temperature and flow experiments, given in tables 5.1 and 5.2. The values of k and E_a, for which the error between model and experimental semi-continuous results was minimized, are represented in table 5.3.

$$r = k \cdot \left(\frac{P_{CO}^{0.5} \cdot P_{H_2}}{P_{CH_3OH}^{0.66}} - \frac{P_{CH_3OH}^{0.34}}{P_{CO}^{0.5} \cdot P_{H_2} \cdot K_{eq}} \right) \quad (5.1)$$

$$k = k_0 \cdot \exp \left(-\frac{E_a}{R \cdot T} \right) \quad (5.2)$$

Figure 5.6 illustrates the conversion of 50 ppm carbon monoxide in hydrogen to methanol, as a function of temperature, at 55 bar and 126 cm³/min (STP), for the semi-continuous experimental results, for the kinetic model generated using Hysys, and for equilibrium data generated using Hysys. As the temperature increases from 100 to 175°C, the equilibrium conversion of carbon monoxide to methanol remains at 100%, after which it decreases to 44% as the temperature increases further to 300°C. As the temperature increases from 154 to 240°C, the experimental conversion of carbon monoxide to methanol increases exponentially from 8% to 48%. As the temperature increases from 100 to 270°C, the conversion of carbon monoxide computed from the kinetic model increases exponentially from 2% to a maximum of 55%. As the temperature increases beyond 270°C, the conversion of carbon monoxide computed from the kinetic model decreases following a similar trend as



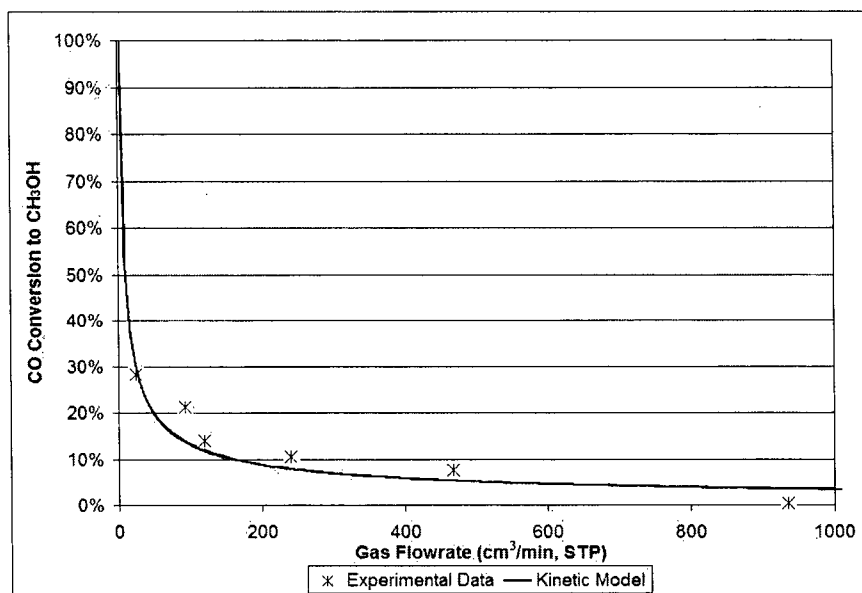
Flowrate 126 cm³/min (STP) and pressure 55 bar

Figure 5.6: Conversion of carbon monoxide to methanol vs. temperature

the equilibrium data, with an offset of approximately 6%, to reach a conversion of carbon monoxide to methanol of 38% at 300°C. The average difference between the experimental conversion of carbon monoxide to methanol and the value computed from the kinetic model is 3.6%.

Figure 5.7 illustrates the conversion of 50 ppm carbon monoxide in hydrogen as a function of feed flowrate, at 180°C and 55 bar for the semi-continuous experimental data and for the kinetic model generated using Hysys. As the flowrate increases from 26 to 935 cm³/min (STP), the experimental conversion of carbon monoxide to methanol decreases exponentially from 28% down to less than 1%. As the flowrate increases from 3 to 935 cm³/min (STP), the conversion of carbon monoxide computed from the kinetic model decreases exponentially from 100% to 4%, while for flowrates below 3 cm³/min (STP) the conversion of carbon monoxide is 100%. The average difference between the experimental conversion of carbon monoxide to methanol and the value computed from the kinetic model is 3.3%.

Applying these results to the use of carbon-11 for the synthesis of [¹¹C]methanol re-



Temperature 180°C and pressure 55 bar

Figure 5.7: Conversion of carbon monoxide to methanol vs. flowrate

quires many considerations. Firstly, the short half life of carbon-11 limits the time allocated to methanol synthesis to less than 5 minutes. Secondly, the [¹¹C]CO would be delivered in approximately 100 cm³ (STP) in hydrogen, which is an order of magnitude less than what was used in the semi-continuous experiments. As illustrated in figure 5.5, the cumulative volume required to release most of the methanol produced is less than 5000 cm³ (STP), which is twice as much as the feed gas volume. Assuming the same correlation applies for the release of [¹¹C]methanol, this would translate to an elution volume of less than 400 cm³ (STP). Together with the 5 minutes time allocated for methanol synthesis, the minimum flowrate would thus be 20 cm³/min (STP). The highest conversion of carbon monoxide to methanol computed from the kinetic model occurs at a temperature at approximately 270°C (figure 5.6). At temperatures above 245°C intra particle diffusion limitations have been observed [80, 79]. Moreover, as illustrated in figure 5.5, at high temperatures the amount of sweep gas required to elute the methanol produced is significantly higher than at temperatures below 224°C. This suggests that the optimal temperature for the carbon-11 application should be around 224°C. At 20cm³/min (STP), 224°C and 55 bar, the kinetic

model predicts a conversion of carbon monoxide to methanol of over 60%.

Chapter 6

Conclusion and Recommendations

6.1 Conclusions

Carbon molecular sieves, in particular when cooled to -20°C , quantitatively trap and release carbon dioxide upon heating to 100°C . A trap has been developed which quantitatively retains and releases $^{11}\text{CO}_2$ in less than 3.5 minutes. Though many existing traps are capable of quantitative trapping, the net advantage of this design lies in its compact size, rapid heating and cooling times, and use of TEC's as opposed to liquid nitrogen. This enables repeated use of the apparatus, without addition of liquid nitrogen. Automation of the system would allow delivery of a semi-continuous supply of $^{11}\text{CO}_2$ for downstream processing, at less than 10 minute intervals.

Carbon dioxide reacts with molybdenum to form molybdenum dioxide and carbon monoxide. Trace amounts of carbon oxides remain adsorbed on reduced molybdenum, and desorb at 800°C , in equilibrium ratios. Reduced, then passivated molybdenum is suitable for reduction of 50 ppm carbon dioxide in helium, to yield carbon monoxide at $800\text{-}880^{\circ}\text{C}$, 2 bar and flow rates under $70\text{ cm}^3/\text{min}$ (STP). Conversions in the order of 70% are possible at these conditions. Aspen, a commercially available process simulator, was used to predict the equilibrium conversion of trace amounts of carbon dioxide to carbon monox-

ide, by reaction with molybdenum. Conversions predicted with this process simulator were consistent with the experimental results.

Trace amounts of carbon monoxide react with hydrogen to form methanol, on a copper zinc oxide catalyst. Reduced, then passivated copper zinc oxide is suitable to catalyze the reaction of 50 ppm carbon monoxide with hydrogen, to form methanol at 180-240°C, 55 bar and 2-935 cm³/min (STP). Based on experimental data, a kinetic model was created using a commercially available process simulator, Hysys. The kinetic model was used to predict optimal operating conditions for practical quantities of [¹¹C]methanol, i.e. over 60% conversion of [¹¹C]carbon monoxide, at 224°C, 55 bar and 20 cm³/min (STP).

6.2 Recommendations for future work

The proposed ¹¹CO₂ trap can be incorporated into any process requiring ¹¹CO₂. However, experiments for ¹¹CO production suggested that the removal of oxygen from the trap was insufficient, using a 30 s helium flush at 200 cm³ (STP) while the trap was at -20°C. It is recommended to flush the trap with helium during the heating step or adding a step in which helium flows through the trap at room temperature to ensure that all the oxygen is removed. This will enable a supply of oxygen free ¹¹CO₂ to the downstream process, avoiding potential contamination with oxygen. When implementing this trap in a process, final adjustments should be done to the helium purge step to ensure that all the oxygen from the target gas is removed.

The proposed molybdenum reactor to convert CO₂ to CO can be readily incorporated in a process requiring ¹¹CO. The experimental results suggest that carbon monoxide and/or carbon dioxide remain adsorbed on the molybdenum surface at ambient temperatures and desorb at about 800°C. Accordingly, care must be taken to remove any traces of ¹²CO₂ or ¹²CO from the molybdenum prior to use for ¹¹CO production, to ensure that this step does not reduce the overall specific activity of the final product. This may be accomplished by

flushing the reactor with UHP helium prior to use, with the reactor heated slightly above operating temperature. The reactor should also remain under inert gas while not used, preferably slightly under pressure, to avoid contamination with carbon-12. Experiments performed with 50 ppm CO₂ indicate that conversions of ¹¹CO₂ to ¹¹CO in the order of 70% are attainable.

The proposed methanol reactor would be suitable to incorporate in a process requiring ¹¹CH₃OH, such as the production of ¹¹CH₃I with high specific activity. The experimental results suggest that carbon monoxide and/or carbon dioxide remained adsorbed on the copper-zinc oxide surface at ambient temperatures and desorb at about 200°C. Accordingly, care must be taken to remove any traces of ¹²CO₂ or ¹²CO prior to catalyst use, to ensure that the final product specific activity remains high. This may be accomplished by flushing the reactor with UHP helium prior to use, with the reactor heated slightly above operating temperature. The reactor should also remain under inert gas while not used, preferably slightly under pressure, to avoid contamination with carbon-12. Based on experimental results obtained using 50 ppm ¹¹CO and the kinetic model, conversion of ¹¹CO to ¹¹CH₃OH in the order of 60% are expected.

Combining the ¹¹CO₂ trap, molybdenum reactor and the gas phase methanol reactor, the entire process has the potential to produce ¹¹CH₃OH in clinically usable quantities. The advantage of the proposed gas phase synthesis over the conventional liquid phase method is the potential to obtain high specific activity carbon-11 radiopharmaceuticals. Further studies with carbon-11 should be done to confirm these projections and to adapt this system to existing PET facilities.

Bibliography

- [1] J. Zessin and P. Mading. Automated Production of [11C]Methyl Iodide. *Forschungszent. Rossendorf, FZR:270*, 1999.
- [2] P.H. Elsinga. Radiopharmaceutical Chemistry for Positron Emission Tomography. *Methods*, 27:208–217, 2002.
- [3] Y. Nishihara, H. Suzuki, and H. Saji. Convenient Production Method of 11C-Labeled Methyl Iodide with High Specific Activity. pages 253–255.
- [4] C. Crouzel and F. Hinnen. Synthesis of [11C]labelled lower chloromethanes: application in methylenation reaction. *J. Label. Comp. Radiopharm.*, 35:92–93 (abstract), 1993.
- [5] J. R. Mallard and C. J. Peachey. Recent Developments in Radioisotope Techniques: a Symposium. IV. A Quantitative Automatic Body Scanner for the Localization of Radioisotopes in Vivo. *Brit. J. Radiol.*, 32:652–7, 1959.
- [6] E. Strajman and N. Pace. In Vivo Studies with Radioisotopes. *Advances in Biol. and Med. Phys.*, 2:194–241, 1951.
- [7] Martin Reivich and Abass Alavi. *Positron emission tomography*. New York : A.R. Liss, 1985.
- [8] Irving Kaplan. *Nuclear Physics*. Cambridge, Mass., Addison-Wesley Pub. Co., 1955.

- [9] J.B. Birks. *Scintillation counters*. London : Pergamon Press Ltd., 1953.
- [10] Henry N Wagner. SNM Highlights As History: 1977. *The Journal of Nuclear Medicine*, pages 35N–37N, 2003.
- [11] Ebco Technologies Inc. Richmond, British Columbia, Canada, 2003.
- [12] Brian Pogue. Medical Imaging. <http://thayer.dartmouth.edu/bpogue/ENGG167/13NuclearMedicine.pdf>.
- [13] C. Crouzel, B. Langstrom, V.W. Pike, and H.H. Coenen. Recommendations for a practical production of [¹¹C] methyl iodide. *Applied Radiation and Isotopes*, 38(8):601–603, 1987.
- [14] Webnox Co. Hyper Dictionary. HyperDictionary.com, 2003.
- [15] Etienne Grech. Positron Emission Tomography, an insight (part 1). Soc. of Med. Radiographers (Malta), http://srm_malta.tripod.com/academia/etienne.htm, 2002.
- [16] K. Hamacher, H.H. Coenen, and G. Stocklin. *J. Nucl. Med.*, 41:49, 1986.
- [17] G. Porenta, J. Czernin, H.R. Schelber, and B.E. Bergmann. Positron emission tomography of the heart. *Futura*, 153-183, 1992.
- [18] A.M.J. Paans, A. van Waarde, P.H. Elsinga, A.T.M. Willemsen, and W. Vaalburg. Positron emission tomography: the conceptual idea using a multidisciplinary approach. *Methods*, 27:195–207, 2002.
- [19] G. Jonkers. Application of C-11, N-13 and O-15 positron emitters for non-intrusive, in situ catalysis research. *Book of Abstracts, 215th ACS National Meeting, Callas, March 29-April 2*, pages COLL–250, 1998.

- [20] B. Langstrom and H. Lundqvist. The preparation of carbon-11-labeled methyl iodide and its use in the synthesis of carbon-11-labeled methionine. *International Journal of Applied Radiation and Isotopes*, 27(7):357–363, 1976.
- [21] P. Larsen, M. Orbe, and K. Dahlstrom. Production of ^{11}C -methyl iodide by monohalogenation of ^{11}C -methane with iodine vapor. *PCT Int. Appl.*, WO 9615086:17 pp., 1996.
- [22] P. Larsen, J. Ulin, K. Dahlstrom, and M. Jensen. Synthesis of ^{11}C iodomethane by iodination of ^{11}C methane. *Applied Radiation and Isotopes*, 48(2):153–157, 1997.
- [23] J.S. Fowler and A.P. Wolf. The synthesis of carbon-11, fluorine-18 and nitrogen-13 labeled radiotracers for biomedical applications. *Nuclear Sciences Series, Nuclear Medicine*, 1982.
- [24] R. Iwata, T. Ido, A. Ujiie, T. Takahashi, K. Ishiwata, K. Hatano, and M. Sugahara. Comparative study of specific activity of ^{11}C methyl iodide: a search for the source of carrier carbon. *Applied Radiation and Isotopes*, 39(1):1–7, 1988.
- [25] D. Comar, C. Crouzel, and B. Maziere. Positron emission tomography: standardization of labeling procedures. *Applied Radiation and Isotopes*, 38(8):587–596, 1987.
- [26] J.M. Link, K.A. Krohn, and J.C. Clark. Production of ^{11}C CH₃I by single pass reaction of ^{11}C CH₄ with I₂. *Nuclear Medicine & Biology*, 24:93–97, 1997.
- [27] G. Berger, C. Prenant, J. Sastre, and D. Comar. Separation of isotopic methanes by capillary gas chromatography. Application to the improvement of methane- ^{11}C specific radioactivity. *International Journal of Applied Radiation and Isotopes*, 34(11):1525–30, 1983.
- [28] K.R. Buckley, J. Huser, S. Jivan, K.S. Chun, and T.J. Ruth. ^{11}C -methane production in small volume, high pressure gas targets. *Radiochim. Acta*, 88:201–205, 2000.

- [29] K. Suzuki, T. Yamazaki, M. Sasaki, and A. Kubodera. Specific activity of $[^{11}\text{C}]\text{CO}_2$ generated in a N_2 gas target: effect of irradiation dose, irradiation history, oxygen content and beam energy. *Radiochimica Acta*, 88(3-4):211–215, 2000.
- [30] Casella et al. Excitation Function for the $^{14}\text{N}(p,\alpha)^{11}\text{C}$ Reaction up to 15 MeV. *Radiochimica Acta*, 25:17–20, 1978.
- [31] G.T. Bida, T.J. Ruth, and P.W. Wolf. Experimentally Determined Thick Target Yields for the $^{14}\text{N}(p,\alpha)^{11}\text{C}$ Reaction. *Radiochimica Acta*, 27:181–185, 1980.
- [32] T. Vandewalle and C. Vandecasteele. Optimisation of the Production of $^{11}\text{C}\text{CO}_2$ by Proton Irradiation of Nitrogen Gas. *Int. J. Appl. Isot.*, 34(10):1459–1464, 1983.
- [33] R. Iwata, T. Ido, Z. Kovacs, and I. Mahunka. A Convenient Cryogenic Trap with Liquid Nitrogen for the Concentration of $[^{11}\text{C}]\text{CO}_2$. *Appl. Radiat. Isot.*, 48(4):483–485, 1997.
- [34] B.H. Mock, M.T. Vavrek, and G.K. Mulholland. Solid-Phase Reversible Trap for $[^{11}\text{C}]\text{Carbon Dioxide}$ Using Carbon Molecular Sieves. *Nucl. Med. Biol.*, 22(5):667–670, 1995.
- [35] R.D. Smith, R.H. Mach, T.E. Morton, B.S. Dembowski, and R.L. Ehrenkauf. Optimization of $[^{11}\text{C}]\text{CO}_2$ Trapping Efficiencies from Nitrogen Gas Streams. *Appl. Radiat. Isot.*, 43(3):466–468, 1992.
- [36] Inc. Alltech Associates. *GC Chromatograms*. 2051 Waukegan Road, Deerfield, IL 60015 USA. Chrom #1063, #1502, 6' 1/8" o.d. 80/100 Carbosphere, 30 ml/min He
Chrom #2222, 6', 1/8" o.d. 80/100 Poropak Q, 30 ml/min He TCD.
- [37] J.C. Clark and P. Buckingham, editors. *Short-Lived Radioactive Gases for Clinical Use*. Butterworths, London, 1975.

- [38] Y. Andersson and B. Langstrom. Synthesis of ^{11}C -Labelled Ketones via Carbonylative Coupling Reactions Using ^{11}C Carbon Monoxide. *J. Chem. Soc., Perkin Trans.*, 1:287–289, 1995.
- [39] A. Suzuki. Synthetic Studies via the Cross-Coupling Reaction of Organoboron Derivatives with Organic Halides. *Pure and Appl. Chem.*, 63:419–422, 1991.
- [40] S.K. Zeisler, M. Nader, A. Theobald, and F. Oberdorfer. Conversion of No_Carrier-Added ^{11}C carbon Dioxide to ^{11}C carbon Monoxide on Molybdenum for the Synthesis of ^{11}C -labelled Aromatic Ketones. *Appl. Radiat. Isot.*, 48(8):1091–1095, 1997.
- [41] B.H. Mock, G.K. Mullholland, and M.T. Tavrek. Convenient Gas Phase Bromination of ^{11}C Methane and Production of ^{11}C Methyl Triflate. *Nuclear Medicine & Biology*, 26:467–471, 1999.
- [42] E. Sarkadi, Z. Kovacs, and L. Ando. Preparation of ^{11}C labeled methyl iodide using aqueous HI adsorbed on alumina. *Radiochimica Acta*, 76:197–200, 1997.
- [43] J.T. Patt. Catalytic conversion of $^{11}\text{C}\text{CO}_2$ and $^{11}\text{C}\text{CO}$ to synthesis precursors for ^{11}C -labeling. *Ber. Forschungszent. Juelich*, page 134 pp., 1994.
- [44] S.D. Jackson, F.E. Hancock, and B.J. Crewdson. Catalytic process. *US patent*, 5,859,070, 1999.
- [45] C. Crouzel and D. Fournier. N.C.A. gas phase production of ^{11}C methanol from ^{11}C methane: application to the online synthesis of $^{11}\text{C}\text{CH}_3\text{I}$. *Sixth Targets and Chemistry Workshop, Vancouver*, pages 314–315, 1995.
- [46] F. Oberdorfer, M. Hanisch, F. Helus, and W. Maier-Borst. A New Procedure for the Preparation of ^{11}C -Labelled Methyl Iodide. *Int. J. Appl. radiat. Isot.*, 36(6):435–438, 1985.

- [47] M. Holschbach and M. Schuller. A New and Simple On-line Method for the Preparation of n.c.a. [11C]Methyl Iodide. *Appl. Radiat. Isot.*, 44(4):779–780, 1993.
- [48] R.F. Sebenik, R.R. Dorfler, J.M. Laferty, and G. Leichtfried. *Molybdenum and Molybdenum Compounds*. Ullmann's Encyclopedia of Industrial Chemistry, 2002.
- [49] Edward I. Stiefel. *Molybdenum Compounds*. Kirk-Othmer Encyclopedia of Chemical Technology, 2001.
- [50] Alfa Aesar. Material safety data sheet, molybdenum (iv) oxide, cas 18868-43-4. Technical report, Health, Safety and Environmental Department, 2005.
- [51] L.V. Belyaevskaya, I.V. Naramosvkii, and N.M. Girdasova. Study of the Kinetics of the Reduction of Sublimated Molybdenum Trioxide. *Sbornik - Moskovskii Instituta Stali i Splavov*, 117:80–85, 1979.
- [52] P.L. Gai. *Phil. Mag.*, A43:841, 1981.
- [53] T. Ressler, R.E. Jentoft, J. Wienold, M.M. Gunter, and O. Timpe. In Situ XAS and XRD Studies on the Formation of Mo Suboxides during Reduction of MoO₃. *J. Phys. Chem. B*, 104:6360–6370, 2000.
- [54] J.S. Lee, S.T. Oyama, and M. Boudart. Molybdenum carbide catalysts: Synthesis of unsupported powders. *Journal of Catalysis*, 106:125–133, 1987.
- [55] Y. Iwasawa and S. Ogaswara. Spectroscopic Study on the Surface Structure and Environment of Fixed Mo Catalysts Prepared by Use of Mo(C₃H₅)₄. pages 1465–1476, 1978.
- [56] R.J. Burch. *J. Chem. Soc., Faraday Trans. 1*, 74:2982, 1978.
- [57] H.M. Spencer and J.L. Justice. The Reaction of Carbon Monoxide on Molybdenum Oxides. *J. Am. Chem. Soc.*, 56:2301–2306, 1934.

- [58] E. Rudy. *Compendium of Phase Diagram Data*. Air Force Materials Laboratory, Wright-Patterson Air Force Base, OH., 1969.
- [59] Alfa Aesar. Material safety data sheet, molybdenum carbide cas 12069-89-5. Technical report, Health, Safety and Environmental Department, 2005.
- [60] S. Dierks. Material data safety sheet, molybdenum carbide. Technical report, ESPI, 1990.
- [61] A. Vandenberghe. Einwirkung einiger Gase auf erhitztes Molybdan. *Z. Anorg. Chem.*, 11:397, 1896.
- [62] S. Hilpert and M. Ornstein. *Ber.*, 46:1669, 1913.
- [63] E.F. Smith and V. Oberholtzer. *J. Am. Chem. Soc.*, 15:206, 1893.
- [64] L. Lian, S.A. Mitchell, and D.M. Rayner. Flow tube kinetic study of mo and mo₂ reactivity. *J. Phys. Chem.*, 98:11637–11647, 1994.
- [65] H. Tulhoff, H. C. Starck Berlin, and W. Goslar. *Carbides*. Ullmann's Encyclopedia of Industrial Chemistry, 2002.
- [66] F. Solymosi, A. Oszko, T. Bansagi, and P. Tolmacsov. Adsorption and Reaction of CO₂ on Mo₂C Catalyst. *J. Phys. Chem. B*, 106:9613–9618, 2002.
- [67] J.C.J. Bart and R.P.A. Sneed. Copper-zinc oxide-alumina methanol catalysts revisited. *Catalysis Today*, 2:1–124, 1987.
- [68] E. Fiedler, G. Grossmann, D. B. Kersebohm, G. Weiss, and C. Witte. *Methanol*. Ullmann's Encyclopedia of Industrial Chemistry, 2002.
- [69] G.C. Chinchin, P.J. Denny, J.R. Jennings, M.S. Spencer, and K.C. Waugh. Synthesis of methanol: Part 1. catalysts and kinetics. *Applied Catalysis*, 36:1–65, 1988.

- [70] K. Klier, V. Chatikavanij, R.G. Herman, and G.W. Simmons. Catalytic synthesis of methanol from CO/H₂: IV. The effects of carbon dioxide. *Journal of Catalysis*, 74(343-360), 1982.
- [71] R.G. Herman, K. Klier, G.W. Simmons, B.P. Finn, J.B. Bulko, and T.P. Kobylinski. Catalytic synthesis of methanol from CO/H₂. i. phase composition, electronic properties, and activities of the Cu/ZnO/Al₂O₃ catalysts. *Journal of Catalysis*, 56:407–429, 1979.
- [72] K. Klier. Methanol Synthesis. *Advances in Catalysis*, 31:243–313, 1982.
- [73] P.J.A. Tijm, F.J. Waller, and D.M Brown. Methanol technology developments for the new millennium. *Applied catalysis A*, pages 275–282, 2001.
- [74] K.C. Waugh. Methanol synthesis. *Catalysis Today*, 15:51–75, 1992.
- [75] S. Zeisler. Personal Communications. 2003.
- [76] Aspen technologies, Aspen process simulator 12.5.
- [77] Hyprotech. Hysys process simulator.
- [78] English A., J. Rovner, J. Brown, and S. Davies. *Kirk-Othmer Encyclopedia of Chemical Technology: Methanol*. John Wiley & Sons, 2005.
- [79] V.E. Leonov, M. Karabaev, E.N. Tsybina, and G.S. Petrishcheva. Study of the kinetics of the methanol synthesis on a low-temperature catalyst. *Kinet. & Katal.*, 14(848-852), 1973.
- [80] G.H. Graaf, H. Scholtens, E.J. Stamhuis, and A.A.C.M. Beenackers. Intra-particle diffusion limitations in low pressure methanol synthesis. *Chemical Engineering Science*, 45, 4:773–783, 1990.
- [81] *Thermochemical properties of inorganic substances*. Springer-Verlag, Berlin, 1973.

Appendix I: Flowmeter calibration curves

The commercially available MKS mass flow controller was calibrated. The mass control valve input voltage was varied from 0-5V, and the output flow of helium was measured using soap-bubble technique. The flowrates were normalized to STP using ideal gas law. The resulting calibration curve is illustrated in figure 6.1, for which a linear trendline was added. The equation relating input voltage signal to actual flow is shown in eq. 6.1, for which the R-squared value was 0.9996 indicating a good correlation.

The 65 mm correlated ball flowmeter, obtained from Cole-Parmer, was calibrated in a similar fashion. The needle valve was adjusted so the reading was 10, 20, 30, 40, 50 and 60. At each point, the flow was measured using soap bubble technique, and adjusted to STP using ideal gas law. The resulting calibration curve is illustrated in figure 6.2, for which a linear trendline was added. The equation relating scale reading to actual flow is shown in eq. 6.2, for which the R-square value was 0.996 indicating a good correlation.

$$F_{MFC}(V_i) = 13.45V_i \quad (6.1)$$

$$F_{CFC}(V_i) = 28.89V_i \quad (6.2)$$

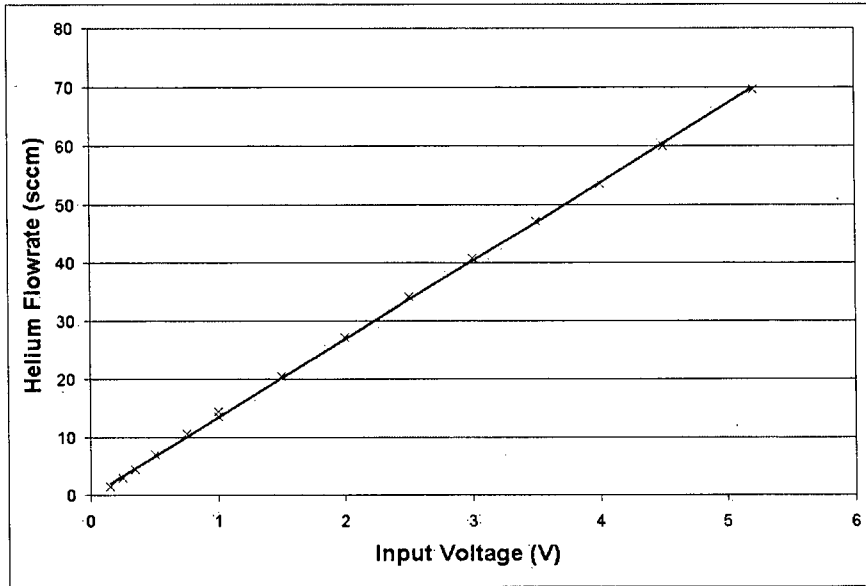


Figure 6.1: Mass flow control valve calibration curve

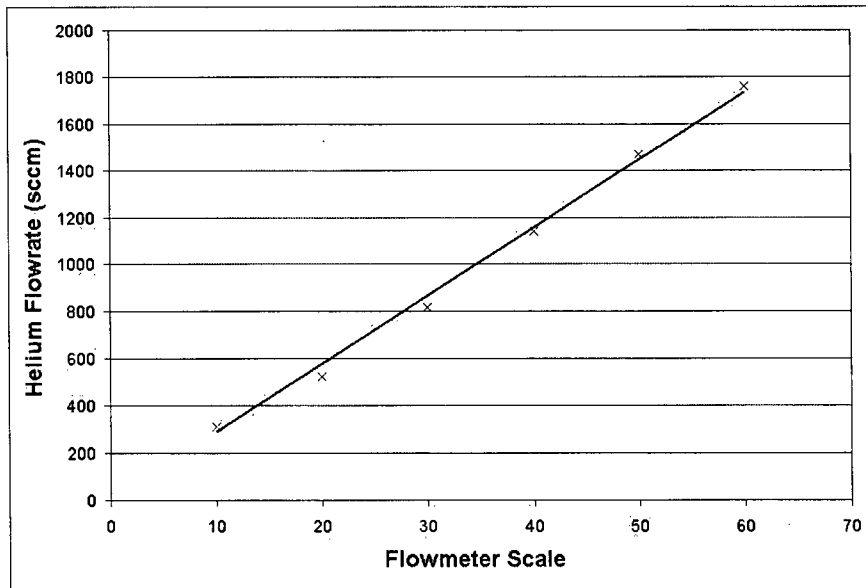
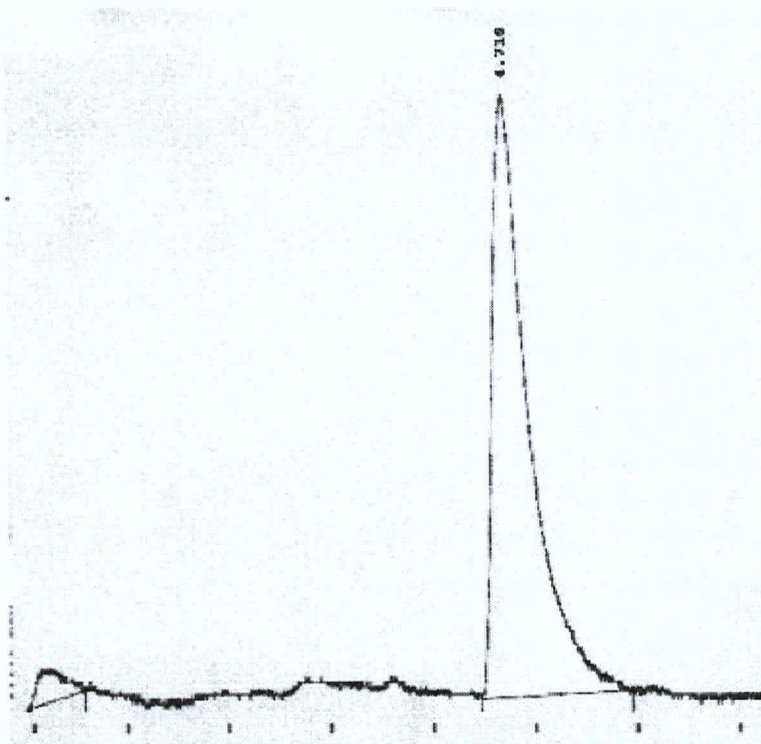


Figure 6.2: Correlated ball flowmeter calibration curve

Appendix II: CO₂, CO, CH₃OH calibration curves

Samples of carbon monoxide, carbon dioxide or methanol were injected in Varian 3600 gas chromatograph equipped with a flame ionization detector and a custom built methanizer. The column used was a 3 m long, 3.2 mm outer diameter, stainless steel tube packed with 60-80 mesh carbon molecular sieve, obtained from Alltech. A typical chromatogram is illustrated in figure 6.3, for a sample containing 50 ppm carbon monoxide.

The calibration curves for carbon dioxide, carbon monoxide and methanol are illustrated in figure 6.4. All three calibration curves show good linearity, with R-squared values over 0.98. Equations relating the peak area to the amount of carbon dioxide, carbon monoxide and methanol are shown in eqs. 6.3, 6.4 and 6.5, respectively. Preliminary calibrations, prior to installation of the methanizer, indicated good linearity between 10 and 500 ppm carbon monoxide. Calibration curves were generated by measuring gas chromatogram peak area of samples containing different amount of either carbon monoxide, carbon dioxide or methanol. The carbon monoxide and carbon dioxide samples were prepared by injecting different volumes of certified gas containing 50 ppm of carbon monoxide or carbon dioxide. Methanol samples were prepared by mixing different ratios of a gas stream saturated with methanol and UHP helium. Based on the temperature, the amount of methanol was calculated, assuming gas stream was saturated with methanol.



Molecular Sieve 13x column, FID Detector, 30 cm³/min (STP) He

Figure 6.3: Gas chromatogram of CO containing sample

$$C_{\text{CO}_2} = 0.00138A + 4.22 \quad (6.3)$$

$$C_{\text{CO}} = 0.00115A - 1.30 \quad (6.4)$$

$$C_{\text{CH}_3\text{OH}} = 0.00166A - 23.6 \quad (6.5)$$

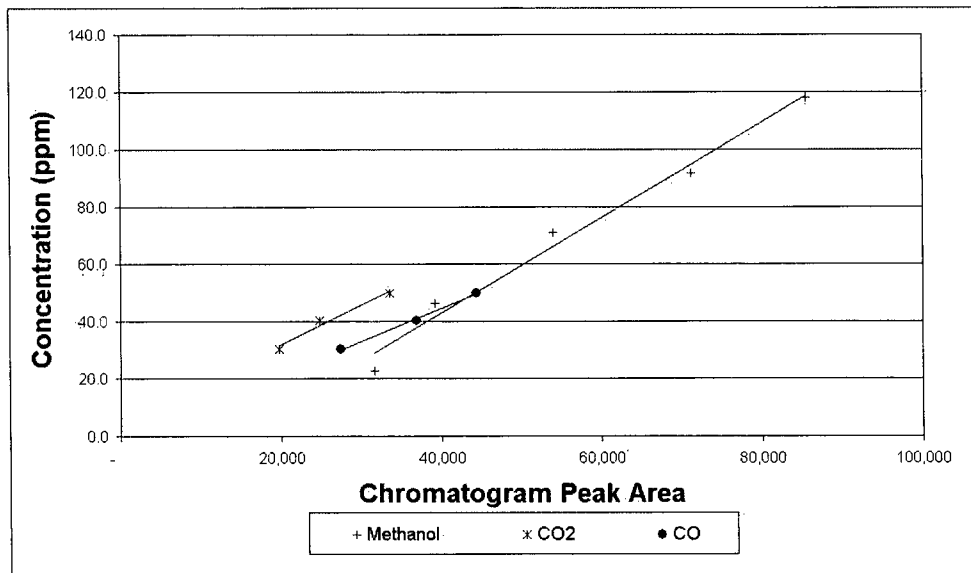


Figure 6.4: CO₂, CO and CH₃OH calibration curves

Appendix III: Surface Molybdenum

During Aspen simulations to obtain equilibrium data for the He, CO, CO₂, C, Mo, MoO, MoO₂, MoO₃, MoC and Mo₂C system, an estimate for required amount of Mo. For equilibrium reactors in Aspen, the reactants must all be specified in the feed stream. Thus, a rough estimate of the amount of Mo present was calculated. The lowest amount available, was calculated assuming that the molybdenum wire is non-porous and thus only molybdenum surface molecules are available for reaction. The highest amount available, was calculated assuming all the molybdenum wire is available for reaction. Table 6.1 illustrates the data used to determine the amount of Mo available for reaction.

Based on the results illustrated in table 6.1 and 6.2, the number of hours the reactor could operate would range from 100 minutes to 4.5 years. The 100 minutes result was obtained assuming that the surface is not porous and that only surface atoms are available

Table 6.1: Mo surface moles rough estimate

Description	value	units
Atomic Radius	0.140	nm
Atomic cross section area	6.16E-20	m ²
Mo wire Surface Area	0.039	m ²
Mo "surface" Atoms	6.4E17	atoms
Mo "surface" moles	1.0E-6	moles
Feed CO ₂	50	ppm
Feed Flowrate	4	sccm
Molar Flowrate CO ₂	1E-8	mole/min
Mo reaction time*	100	min

*Assuming 100% Mo conversion to MoO₂

Table 6.2: Mo total moles

Description	value	units
Molecular Weight	95.94	g/mole
Weight Mo used in reactor	2.2385	g
Mo total moles	0.023	moles
Feed CO ₂	50	ppm
Feed Flowrate	4	sccm
Molar Flowrate CO ₂	1E-8	mole/min
Mo reaction time*	4.5	years

*Assuming 100% Mo conversion to MoO₂

for reaction. Typically reactions take place for less than five minutes per synthesis. Molybdenum being in excess of CO₂ in the reactant stream is thus a reasonable assumption.

Appendix IV: Temperature Profile

The temperature profile was measured for the molybdenum reactor with open ends and for the reactor with quartz wool plugged ends, with a temperature setpoint of 740°C. The position of a K-type thermocouple was moved from one end to the other of the reactor, monitoring the temperature each 2 cm. As illustrated in figure 6.5, the addition of quartz wool plugs improves the temperature gradient. The molybdenum was placed across a 10 cm length, from $L = 2\text{cm}$ to $L=12\text{ cm}$. Over this length, the temperature varies from approximately 580°C to 740°C for the open ended reactor, and from approximately 680°C to 740°C for the plugged ends reactor. Thus the net effect of the quartz wool plugs was to reduce the temperature variance from 160°C to 60°C.

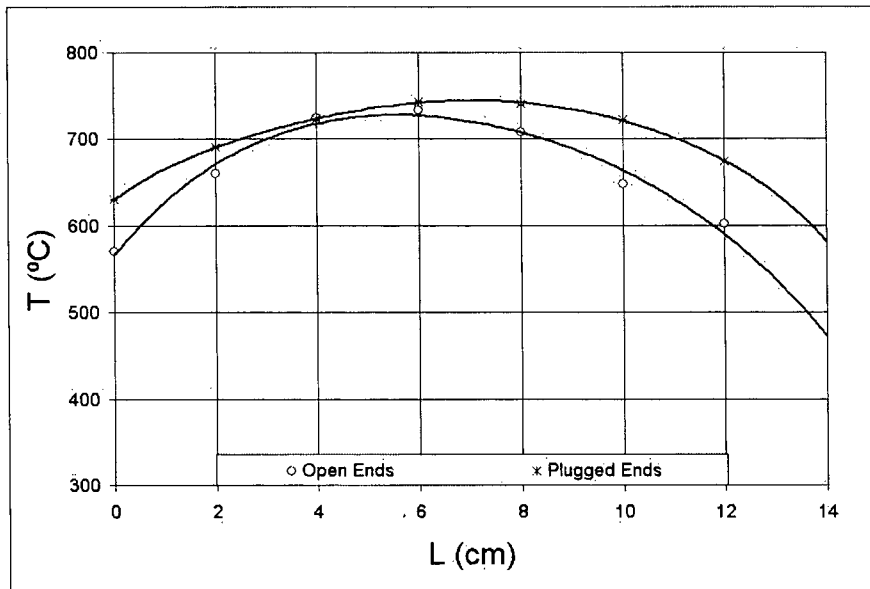


Figure 6.5: Reactor temperature profile, at 740°C

Appendix V: Process simulator

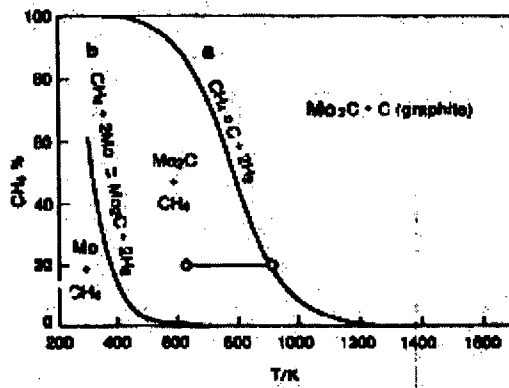
Hysys is suitable for mainly gas/liquid phase reactions, with possible solid products. Carbon exists in the Hysys database while other solids can be custom created. Since Aspen has a built in database containing many solid compounds, including molybdenum, it was selected to carry out the equilibrium reactions. First, to validate the simulator, Aspen generated equilibrium data was compared to those reported in literature, for the reactions of methane with molybdenum and hydrogen with carbon.

We can see in figures 6.7 and 6.6 that the equilibrium relationships generated using Aspen are quite similar to those reported [81]. The equilibrium curves for the formation of dimolybdenum carbide follow a similar pattern, however there is an offset on the temperature scale of about 25 K. The equilibrium curves for the formation of dimolybdenum carbide follows a similar pattern, however there is an offset on the temperature scale of about 100 K. Although the temperature difference is significant, the shape of the curves are near identical. Thus Aspen was used to generate equilibrium curves. The following description represents the steps required to set-up an Aspen simulation to obtain equilibrium data for the Mo, MoO, MoO₂, MoO₃, CO₂, CO, O₂, C system. Equilibrium curves generated for other component systems follow a similar procedure and differ only in the components used, temperature range and pressure range.

1. Setup

Units: SI

Stream Class: MIXCISLD, for use when conventional solids are present with no



- (a) $CH_4 \rightleftharpoons C_{(s)} + 2H_2$
 (b) $CH_4 + 2 \cdot Mo \rightleftharpoons Mo_2C + 2H_2$
 Obtained from [81]

Figure 6.6: Equilibrium relationships at atmospheric pressure Mo-C-Mo₂C-H₂-CH₄

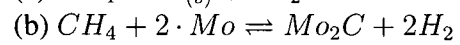
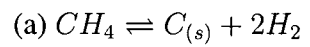
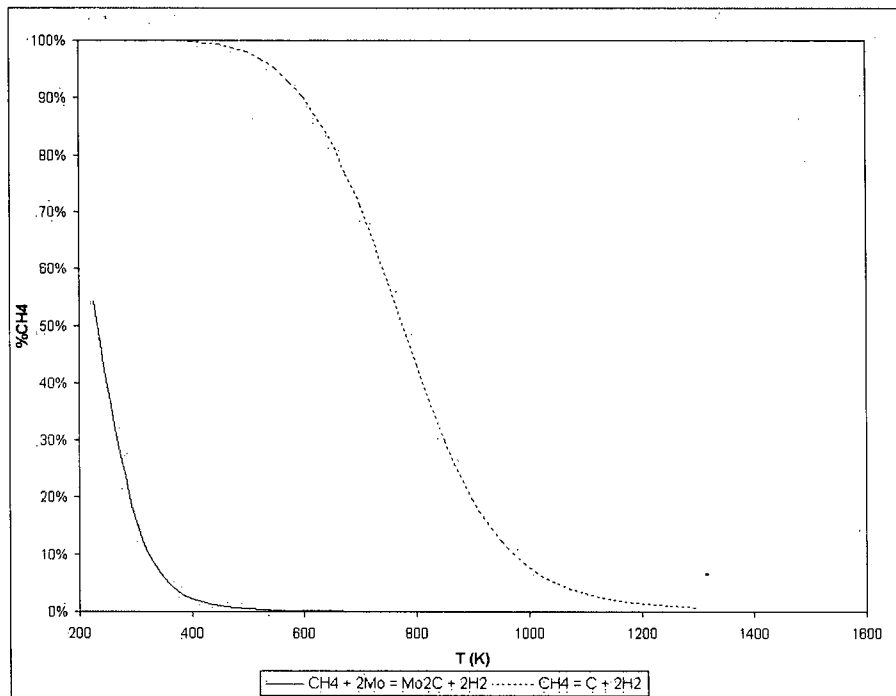


Figure 6.7: Aspen generated equilibrium relationships at atmospheric pressure Mo-C-Mo₂C-H₂-CH₄

particle size distribution.

2. Possible Components:

To begin with, here is a list of the compounds that can be present in the system, based on a feed of CO_2 through a reactor containing Mo. Solids need to be defined as type solid in Aspen, while gases are defined as type conventional

Conventional: CO_2 , CO, O_2 , Ar

Solid: Mo, C, MoO, Mo_2O_3 , MoO_2 , Mo_2O_5 , MoO_3 , Mo_2C , MoC

Note: Components Mo_2O_3 , Mo_2O_5 not part of database.

3. Properties

Base Method: Peng-Robinson

4. Create Gibbs Reactor, with a feed stream and an equilibrium stream

Set temperature: 273 K

Set pressure: 2 bar

5. Define Feed stream

Set composition of feed to desired mole fraction of each component

Set temperature: 273 K

Set pressure: 2 bar

Set flowrate: 1 mole/sec

6. Model Analysis Tools

Sensitivity

Create new sensitivity analysis

Define variables: all components in equilibrium stream in terms of mole fractions

Temperature range 273-1573 K, 150 data points

The molar flow rate for each component was tabulated, copied to excel. From molar flowrate, molar fractions were easily calculated and plotted.

APPENDIX VI: Estimation of CO₂ concentrations

The exact amount of CO₂ contained in the target gas at Sherbrooke facilities is unknown. Sherbrooke facilities are not set-up to measure specific activity and by no means require high specific activity for their use of carbon-11. Thus, their system is not optimized and no special precautions were taken to obtain high specific activity from their target. The range of reported specific activities is 0.1-16.5 Ci/μmol [45, 1, 21]. In practice, between 200-1000 mCi ¹¹CO₂ will be produced for each clinical run. During experiments at the CHUS, 250 mCi was produced each run. The content of CO₂ entering the molybdenum reactor can be estimated based on the flowrate of pushed used and the time required to eluted all the ¹¹CO₂. As can be seen in table 6.3, this corresponds to between 28-560 ppm CO₂.

The time required to elute all the ¹¹CO₂ is estimated to be between 2-5 minutes, at flowrates between 25-200 cm³/min and a pressure of 2 bar. This corresponds to a broad range of CO₂ concentrations, roughly between 1 and 2,000 ppm CO₂, as can be seen in table 6.3. Gases containing 50 ppm of CO₂ or 50 ppm CO were selected to represent quantities used in routine carbon-11 radiopharmaceutical synthesis.

Table 6.3: CO₂ concentration estimates

	SA (Ci/μmol)	¹¹ CO ₂ (mCi)	umol CO ₂	Q (c ³ m/min)	P (bar)	t (min)	ppm CO ₂
CHUS	0.1	250	2.5	25-200	2	2-5	28-560
Low SA	0.1	200-1000	2-10	25-200	2	2-5	22-2,200
High SA	16.5	200-1000	0.01-0.06	25-200	2	2-5	0.7-27